Hindawi
Structural Control and Health Monitoring
Volume 2023, Article ID 6906855, 19 pages
https://doi.org/10.1155/2023/6906855

Research Article

Vehicle Scanning Method for Bridges Enhanced by Dual Amplifiers

Hao Xu,[1,2] **M. Yang**,[1,2] **Judy P. Yang**,[3] **Z. L. Wang**,[1,2] **K. Shi**,[1,2] **and Y. B. Yang**[1,2,4]

[1]*School of Civil Engineering, Chongqing University, Chongqing 400045, China*
[2]*MOE Key Laboratory of New Technology for Construction of Cities in Mountain Area, Chongqing University, Chongqing, China*
[3]*Department of Civil Engineering, National Yang Ming Chiao Tung University, Hsinchu 300093, Taiwan*
[4]*School of Civil Engineering and Architecture, Chongqing University of Science and Technology, Chongqing 401331, China*

Correspondence should be addressed to Judy P. Yang; jpyang@nycu.edu.tw and Y. B. Yang; ybyang@cqu.edu.cn

Received 28 October 2022; Revised 2 May 2023; Accepted 6 May 2023; Published 22 May 2023

Academic Editor: Lin Chen

Dual-function amplifiers are proposed for the first time herein for enhancing the capability of a scanning test vehicle for bridges. To start, closed-form solutions are derived for the dynamic responses of the amplifier-vehicle-bridge system with a moving test vehicle. Then, the dynamic amplification factors of the amplifier and vehicle are presented for assessing the bridge/vehicle and vehicle/amplifier transmissibility. It was known that the spectrum of the vehicle may be hindered for extracting the bridge frequencies because of *vehicle frequency and rough pavement*. Two differentially tuned amplifiers are called on to tackle the problem: one (i.e., the vehicle damper) is to *suppress the effect of vehicle's frequency*, acting like the tuned mass damper (TMD), and the other (i.e., the bridge amplifier) is to *enlarge the amplitude of bridge frequency* of concern. Based on the parametric study, it is concluded that (1) the bridge amplifier performs better than the vehicle one in extracting bridge frequencies by increasing their visibility in the spectrum; (2) the effect of vehicle's frequency can be suppressed by tuning the vehicle damper such that it functions like a TMD of the vehicle; (3) by tuning the bridge amplifier to any of the first few bridge frequencies, the latter can be well detected even for rough pavement.

1. Introduction

In transportation networks, bridges play a critical role in connecting roads that are separated by natural or artificial barriers. They are vital to the performance of civil infrastructure and also to the economic development of a region or country. For this reason, bridges have received continuous attention from researchers and engineers concerning their safety and reliability. Previously, vibration-based structural health monitoring methods have been widely employed to provide reference data to the bridge administrators for duty scheduling and decision making [1–7]. Conventionally, the *direct method* that relies on the data collected from sensors *directly* installed on the bridge has been frequently used. However, such an approach suffers from the drawbacks including high cost in implementation and maintenance, difficulty in digesting the continuously generated data, lack of movability for the hardware system tailored for one bridge, and short service life of the electronic devices installed compared with that of the bridge. Therefore, except for strategically important or structurally special bridges, the direct approach with fixed sensors has not been considered an effective approach for bridge monitoring. On the other hand, there exist a huge number of bridges in the world that are faced with problems of ageing, overloading, deterioration, etc. but have not received adequate care from structural health monitoring. Clearly, there is an urgent need to develop an economical and efficient method to monitor the vast amount of bridges.

As part of the effort to meet the above need, a moving test vehicle fitted with an accelerometer was proposed for extracting the frequencies of bridges by Yang et al. [8] in 2004. Such an approach rooted in the vehicle-bridge interaction (VBI) and originally known as the *indirect method*

was later renamed as the *vehicle scanning method* (VSM) for bridges for better conveyance of the meaning implied. Primarily, the dynamic responses of the moving test vehicles were used for scanning the bridge frequencies [8–14]. The technique was then extended to identification of other properties of the bridge, such as the mode shapes [15–28], damping ratios [29, 30], and damage [31–37]. Over the years, the merits of the VSM for scanning bridge modal properties have been verified by experimental and field tests [9, 14, 18, 20]. As a matter of fact, the VBI in general and the VSM in particular are problems that deserve further investigation, as pointed out in some recent papers and reviews in [38–41].

The successful application of the VSM relies on both the software and hardware sides. On the software side, an effective signal processer is essential to the extraction of bridge dynamic properties. To extract bridge frequencies of the higher modes, the empirical mode decomposition (EMD) and variants were adopted to decompose the collected signals into intrinsic mode functions (IMFs) [42–45]. In this regard, the mode mixing problem was resolved by the variational mode decomposition (VMD) with a band-pass filter [46]. Besides, techniques such as Hilbert transform [15, 17, 21, 26, 27], short time frequency domain decomposition [16], stochastic subspace identification [19], matrix completion [23], and wavelet [24] were used for constructing bridge mode shapes. To improve the efficiency of the VSM, some automatic modal identification techniques were also adopted [47, 48].

As far as the vehicle response is concerned, it is annoying that the *vehicle's self-frequency* often appears too outstanding for the bridge frequencies to be identified from the spectrum. To tackle this problem, methods such as the particle filter [49], vehicle-bridge contact response algorithm [27, 50, 51], and matrix completion [25, 52] were introduced to remove the frequency or to reduce the suspension effect of the test vehicle.

On the hardware side, it is crucial to develop a test vehicle with proper dynamic properties for signal collection. Previously, the test vehicle was designed as a *single-axle* trailer for its resemblance with the *single-degree-of-freedom (DOF) system* used in theoretical formulations [8]. Such a simple vehicle model allows the mechanism of interaction between the moving test vehicle and the bridge to be clearly interpreted and has been widely employed in theoretical and numerical studies [12, 15, 21, 33, 34, 42, 44, 50]. Previously, research studies have been conducted to consider various properties of the single-axle test vehicle, including the rocking motion [53, 54], suspension effect, and cogwheel load effect [10, 51, 55, 56].

For a test vehicle that is well designed, there remains another problem to face, i.e., the *pavement roughness* of the bridge to be measured. Previous research has indicated that the high-frequency disturbances induced by rough pavements may pollute the vehicle spectrum, thereby rendering it difficult to identify the bridge frequencies. Attempts that have been made to alleviate such an effect include cross-spectral density function estimation [57], second-order blind identification (SOBI) [22], and vehicle-bridge contact residual [27].

On the other hand, it has been demonstrated that the test vehicle can be improved through the addition of an amplifier to the test vehicle [58]. Both the test vehicle and amplifier are fitted with accelerometers. The amplifier (or associated accelerometer) can be mounted at the tip of a cantilever that is rigidly connected to the vehicle body (or axle), of which the damping can be ignored. In addition, the arm length of the cantilever can be adjusted by a screw device, by which the frequency of the amplifier can be tuned to the vehicle frequency or any of the bridge frequencies. It should be noted that the frequencies identified for the vehicle-amplifier system should be taken as the eigenfrequencies of the system. In practice, however, the amplifier is designed to be very light compared with the test vehicle. Thus, the difference between the eigenfrequencies and vehicle/amplifier frequencies are negligible. For convenience, terms such as vehicle's (self) frequency and amplifier frequency, rather than eigenfrequencies, will still be used for easy communication.

From the above review, it is clear that for the vehicle scanning method to be successful, two issues should be properly dealt with, i.e., the *self-frequency* of the test vehicle and *pavement roughness* of the bridge to be measured. Quite often the vehicle's self-frequency may have such an outstanding magnitude relative to those of the bridge's frequencies that the latter are hidden in the vehicle spectrum. In addition, for a test vehicle moving at *high speeds*, the roughness-related *high-frequency noise* may be induced by the pavement, which tends to mask the bridge frequencies of the higher modes.

This theoretical paper is aimed at *simultaneously* tackling the above two issues by proposing the installation of *dual amplifiers* on the test vehicle, from the hardware aspect. One amplifier will be tuned to the frequency of the test vehicle (referred to as the *vehicle damper*), to serve as a tuned mass damper (TMD) for suppressing the effect of vehicle's frequency. The other amplifier will be tuned to the bridge frequency of interest (referred to as the *bridge amplifier*) to amplify its magnitude in the spectral response. The second amplifier offers some alleviation on the noise induced by pavement roughness.

The vehicle scanning method is not a "hit-and-go" technique but an "iterative process" for a successful bridge test. Aside from the pretest as a prerequisite for obtaining the basic vehicle properties, the test vehicle will be allowed to travel over the bridge for a couple of *test runs*, of which the total time consumed is reasonably low, depending on the experience of the practitioner. During the test runs, rough data will be gained of the bridge for use in tuning the vehicle parameters. Based on the data acquired in the test runs, the two amplifiers (which are adaptive) can be generally tuned (or optimized) to meet the practical needs. In particular, the vehicle damper should be tuned for the vehicle frequency, in order to minimize the vehicle's disturbance. Meanwhile, the bridge amplifier should be tuned to any of the first few frequencies of the bridge, by which the maximum visibility can be achieved for the frequencies of concern, including the 2^{nd} and 3^{rd} ones. All the above adjustments for the amplifiers can be conducted in an iterative or trial-and-error manner.

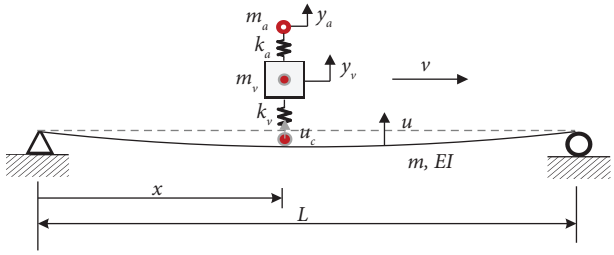

Figure 1: Amplifier-vehicle-bridge system.

This paper is outlined as follows. In Section 2, the closed-form solutions of the dynamic responses of the system are derived. In Section 3, the *dynamic amplification factors* (DAFs) of the amplifier and vehicle for the bridge response, concerning the tuning and featured range of the amplifier, will be investigated. In Section 4, the amplifier-vehicle-bridge interaction element for dual amplifiers will be presented, and the analytical solutions will be verified by the finite element method (FEM). In Section 5, phenomena such as the resonance and cancellation of the amplifier-vehicle system will be numerically investigated. In Section 6, a parametric study will be conducted for the effects of mass and frequency of the amplifier, pavement roughness, and dual amplifiers. In Section 7, the applicability of dual amplifiers will be numerically assessed. Finally, concluding remarks are given in Section 8.

2. Analytical Formulation of the Problem

In this section, the analytical formulation of the whole system including the *amplifier*, vehicle, and bridge will be presented. For the present purposes, a simply supported beam is considered in the derivation of closed-form solutions, but it is known that the VSM can be applied to other types of bridges as well, such as multi-span bridges [27, 59], curved bridges [60], and bridges with non-simply supported conditions [61]. To enable derivation of concise closed-form solutions for the amplifier-vehicle-bridge system, it is assumed that the mass of the test vehicle is very small compared with that of the bridge. Consequently, the action of the test vehicle on the bridge can be treated as a moving load neglecting the effect of the vehicle-bridge interaction (VBI), namely, ignoring the inertial effect of the test vehicle on the bridge response.

2.1. Dynamic Responses of the Bridge. As shown in Figure 1, a simple beam is subjected to a moving test vehicle equipped with an amplifier. The test vehicle is modeled as a concentrated mass m_v supported by a spring k_v, and the amplifier is modeled as a (much smaller) concentrated mass m_a connected to the vehicle body by a spring k_a. The frequency of the amplifier is tunable since its spring stiffness can be easily adjusted. The bridge considered is an Euler-Bernoulli beam of span length L, per-unit-length mass m, and flexural stiffness EI. The test vehicle adopted is a single-axle or single-DOF vehicle, which has been extensively used in previous theoretical and experimental studies for its close resemblance between the theoretical formulation and physical model and for better interpretation of the physical phenomena observed [8, 9, 12–14]. To obtain closed-form solutions of the amplifier-vehicle-bridge system for unveiling the mechanism involved, the damping of the whole system is ignored.

The equations of motion for the amplifier, test vehicle, and bridge are

$$m_a \ddot{y}_a + k_a (y_a - y_v) = 0, \tag{1}$$

$$m_v \ddot{y}_v + k_v (y_v - u_c) + k_a (y_v - y_a) = 0, \tag{2}$$

$$m\ddot{u} + EIu'''' = f_c(t)\delta(x - vt), \tag{3}$$

where y_a and y_v denote the displacements of the amplifier and test vehicle, respectively; u and u_c are those of the beam and the contact point, with $u_c = u|_{x=vt}$; a dot ($\dot{}$) and prime ($'$) denote a time and spatial derivatives; δ denotes Dirac's delta function. It should be noted that the displacements of the amplifier and vehicle, i.e., y_a, and y_v, are measured with respect to the static equilibrium positions. The contact force f_c imposed on the bridge in equation (3) is

$$f_c(t) = k_v (y_v - u_c) - (m_v + m_a) g, \tag{4}$$

where g is the acceleration of gravity.

The vertical displacement of the beam u can be replaced by the modal superposition [62]:

$$u(x,t) = \sum_n q_{b,n}(t) \sin \frac{n\pi x}{L}, \tag{5}$$

where $q_{b,n}$ is the n^{th} modal displacement of the beam. By assuming the vehicle mass m_v and amplifier mass m_a to be much less than the bridge mass mL (i.e., $(m_v + m_a) \ll mL$) [63], one can substitute equation (5) into equation (3), multiplying both sides by $\sin(n\pi x/L)$ and integrating along the span length L to arrive

$$\ddot{q}_{b,n}(t) + \omega_{b,n}^2 q_{b,n}(t) = \frac{-2(m_v + m_a) g}{mL} \sin \frac{n\pi v t}{L}, \tag{6}$$

where $\omega_{b,n}$ is the n^{th} modal frequency:

$$\omega_{b,n} = \frac{n^2 \pi^2}{L^2} \sqrt{\frac{EI}{m}}. \tag{7}$$

For the beam with zero initial conditions (i.e., $q_{b,n}(0) = 0$ and $\dot{q}_{b,n}(0) = 0$), the n^{th} modal displacement of the beam in equation (6) can be obtained:

$$q_{b,n}(t) = \frac{\Delta_{st,n}}{1 - S_n^2} \left[\sin\left(\frac{n\pi v t}{L}\right) - S_n \sin\left(\omega_{b,n} t\right) \right], \tag{8}$$

where $\Delta_{st,n}$ is the n^{th} modal static deflection caused by $(m_v + m_a)g$, and S_n is the speed parameter. They are defined below:

$$\Delta_{st,n} = \frac{-2(m_v + m_a) g L^3}{n^4 \pi^4 EI}, S_n = \frac{n\pi v}{L\omega_{b,n}}. \tag{9}$$

Substituting equation (8) into equation (5), one can obtain the displacement of the beam $u(t)$ as

$$u(x,t) = \sum_n \frac{\Delta_{st,n}}{1-S_n^2}\left[\sin\left(\frac{n\pi vt}{L}\right) - S_n \sin\left(\omega_{b,n}t\right)\right]\sin\frac{n\pi x}{L}. \tag{10}$$

By letting $x = vt$ in equation (10) and using trigonometric function formulas, one arrives at the *contact response* as

$$u_c(t) = \sum_n \frac{\Delta_{st,n}}{2\left(1-S_n^2\right)}\left\{1 - \cos\left(\omega_{d,n}t\right) - S_n\left[\cos\left(\omega_{bl,n}t\right) - \cos\left(\omega_{br,n}t\right)\right]\right\}, \tag{11}$$

where the *driving frequency* $\omega_{d,n}$ and two *shifted bridge frequencies* $\omega_{bl,n}$ and $\omega_{br,n}$ are

$$\omega_{d,n} = \frac{2n\pi v}{L}, \omega_{bl,n} = \omega_{b,n} - \frac{n\pi v}{L}, \omega_{br,n} = \omega_{b,n} + \frac{n\pi v}{L}. \tag{12}$$

2.2. Dynamic Responses of the Amplifier and Test Vehicle. The equations of the amplifier and test vehicle in equations (1) and (2) can be combined:

$$\begin{bmatrix} m_a & 0 \\ 0 & m_v \end{bmatrix}\begin{bmatrix} \ddot{y}_a \\ \ddot{y}_v \end{bmatrix} + \begin{bmatrix} k_a & -k_a \\ -k_a & (k_v + k_a) \end{bmatrix}\begin{bmatrix} y_a \\ y_v \end{bmatrix} = \begin{bmatrix} 0 \\ k_v u_c \end{bmatrix}. \tag{13}$$

By letting $\mathbf{K}$ and $\mathbf{M}$ denote the stiffness and mass matrices in equation (13), respectively, the frequencies of the whole system can be solved by letting $\|\mathbf{K} - \omega^2\mathbf{M}\| = 0$:

$$\omega_i^2 = \frac{\omega_a^2 + \omega_v^2 + \omega_a^2 m_a/m_v \pm \sqrt{\left(\omega_a^2 + \omega_v^2 + \omega_a^2 m_a/m_v\right)^2 - 4\omega_a^2\omega_v^2}}{2}, i = 1, 2, \tag{14}$$

where

$$\omega_a = \sqrt{\frac{k_a}{m_a}}, \tag{15}$$

$$\omega_v = \sqrt{\frac{k_v}{m_v}}. \tag{16}$$

Substituting u_c given in equation (11) into equations (1) and (2) and assuming the amplifier and test vehicle to start from rest (i.e., $y_a(0) = 0$, $\dot{y}_a(0) = 0$, $y_v(0) = 0$, and $\dot{y}_v(0) = 0$), the displacements of the amplifier and test vehicle can be solved as

$$y_a(t) = \sum_n \frac{\Delta_{st,n}}{2\left(1-S_n^2\right)}\left\{\begin{array}{c} 1 - A_{1,n}\cos\left(\omega_1 t\right) + A_{2,n}\cos\left(\omega_2 t\right) \\ -A_{d,n}\cos\left(\omega_{d,n}t\right) - S_n\begin{bmatrix} A_{bl,n}\cos\left(\omega_{bl,n}t\right) \\ -A_{br,n}\cos\left(\omega_{br,n}t\right) \end{bmatrix} \end{array}\right\}, \tag{17}$$

$$y_v(t) = \sum_n \frac{\Delta_{st,n}}{2\left(1-S_n^2\right)}\left\{\begin{array}{c} 1 - V_{1,n}\cos\left(\omega_1 t\right) + V_{2,n}\cos\left(\omega_2 t\right) \\ -V_{d,n}\cos\left(\omega_{d,n}t\right) - S_n\begin{bmatrix} V_{bl,n}\cos\left(\omega_{bl,n}t\right) \\ -V_{br,n}\cos\left(\omega_{br,n}t\right) \end{bmatrix} \end{array}\right\}, \tag{18}$$

where the coefficients are as follows (with coefficient A for amplifier and coefficient V for vehicle):

$$A_{1,n} = \frac{\left(\omega_a^2 - \omega_2^2\right)\widetilde{A} - \omega_a^2\widetilde{V}}{\left(\omega_1^2 - \omega_2^2\right)},$$

$$A_{2,n} = \frac{\left(\omega_a^2 - \omega_1^2\right)\widetilde{A} - \omega_a^2\widetilde{V}}{\left(\omega_1^2 - \omega_2^2\right)},$$

$$A_{d,n} = \frac{\alpha_{v,a}\beta_{v,a}}{\left(\alpha_{v,a}\omega_{d,n}^2/\omega_a^2 - \alpha_{v,a}\beta_{v,a} - 1\right)\left(\omega_{d,n}^2/\omega_a^2 - 1\right) - 1},$$

$$A_{bl,n} = \frac{\alpha_{v,a}\beta_{v,a}}{\left(\alpha_{v,a}\omega_{bl,n}^2/\omega_a^2 - \alpha_{v,a}\beta_{v,a} - 1\right)\left(\omega_{bl,n}^2/\omega_a^2 - 1\right) - 1},$$

$$A_{br,n} = \frac{\alpha_{v,a}\beta_{v,a}}{\left(\alpha_{v,a}\omega_{br,n}^2/\omega_a^2 - \alpha_{v,a}\beta_{v,a} - 1\right)\left(\omega_{br,n}^2/\omega_a^2 - 1\right) - 1},$$

$$V_{1,n} = \left(1 - \frac{\omega_1^2}{\omega_a^2}\right)A_{v1,n},$$

$$V_{2,n} = \left(1 - \frac{\omega_2^2}{\omega_a^2}\right)A_{v2,n},$$

$$V_{d,n} = \frac{\alpha_{v,a}\beta_{v,a}\left(1 - \omega_{d,n}^2/\omega_a^2\right)}{\left(\alpha_{v,a}\omega_{d,n}^2/\omega_a^2 - \alpha_{v,a}\beta_{v,a} - 1\right)\left(\omega_{d,n}^2/\omega_a^2 - 1\right) - 1},$$

$$V_{bl,n} = \frac{\alpha_{v,a}\beta_{v,a}\left(1 - \omega_{br,n}^2/\omega_a^2\right)}{\left(\alpha_{v,a}\omega_{bl,n}^2/\omega_a^2 - \alpha_{v,a}\beta_{v,a} - 1\right)\left(\omega_{bl,n}^2/\omega_a^2 - 1\right) - 1},$$

$$V_{br,n} = \frac{\alpha_{v,a}\beta_{v,a}\left(1 - \omega_{br,n}^2/\omega_a^2\right)}{\left(\alpha_{v,a}\omega_{br,n}^2/\omega_a^2 - \alpha_{v,a}\beta_{v,a} - 1\right)\left(\omega_{br,n}^2/\omega_a^2 - 1\right) - 1}, \tag{19}$$

along with the mass ratio $\alpha_{v,a}$ and frequency ratio $\beta_{v,a}$ as

$$\alpha_{v,a} = \frac{m_v}{m_a}, \beta_{v,a} = \frac{\omega_v^2}{\omega_a^2}, \tag{20}$$

$$\widetilde{A} = 1 - A_{d,n} - S_n A_{bl,n} + S_n A_{br,n}, \tag{21}$$

$$\widetilde{V} = 1 - V_{d,n} - S_n V_{bl,n} + S_n V_{br,n}. \tag{22}$$

The accelerations of the amplifier $\ddot{y}_a(t)$ and vehicle $\ddot{y}_v(t)$ can be obtained by differentiating equations (17) and (18) twice, which are not shown here for brevity. Of interest is that since different vibration components (i.e., those related to the driving and shifted bridge frequencies in the contact response) are transmitted from the contact point to the vehicle and then to the amplifier through the same transmission mechanism, the coefficients ($A_{d,n}$, $A_{bl,n}$, $A_{br,n}$) in the amplifier response in equation (17) and the coefficients ($V_{d,n}$, $V_{bl,n}$, $V_{br,n}$) in the vehicle response in equation (18) are identical in form.

3. Effect of Amplifier on the Amplifier-Vehicle-Bridge System

The purpose of using the amplifier is twofold: one (i.e., using the bridge amplifier) is to amplify the bridge frequency of concern and the other (i.e., using the vehicle damper) is to suppress the effect of vehicle's frequency, which may overshadow the bridge frequencies in the vehicle spectrum. Both will be studied in the following.

3.1. Dynamic Amplification Factor of Amplifier for the Bridge Response. For the first purpose, the *dynamic amplification factor* (DAF) of the *amplifier* for the bridge response is defined as the ratio of the amplitude of each excitation frequency (i.e., driving frequency $\omega_{d,n}$ or shifted bridge frequencies $\omega_{bl,n}$ and $\omega_{br,n}$) in the amplifier response in equation (17) to that in the contact response in equation (11), namely,

$$\mathrm{DAF}_a\left(\alpha_{v,a}, \beta_{v,a}, \beta_{i,a}\right) = A_{i,n} = \left|\frac{\alpha_{v,a}\beta_{v,a}}{\left(\alpha_{v,a}\beta_{i,a} - \alpha_{v,a}\beta_{v,a} - 1\right)\left(\beta_{i,a} - 1\right) - 1}\right|, \tag{23}$$

where subscript i can be (d, n), (bl, n), or (br, n), and $\beta_{i,a}$ is a frequency ratio defined as

$$\beta_{i,a} = \frac{\omega_i^2}{\omega_a^2}. \tag{24}$$

Of interest is that the amplifier's DAF_a for each frequency of interest is identical to the amplifier's coefficient $A_{i,n}$. It should be noted that in deriving the amplifier's DAF_a equation in (23), no assumption was made regarding the smallness of the amplifier mass with respect to the vehicle mass (i.e., $m_a \ll m_v$). In practice, however, the amplifier mass is *very small* compared with the vehicle mass. Therefore, to facilitate the discussion, the curve of the DAF_a with respect to $\beta_{v,a}$ and $\beta_{i,a}$ is plotted in Figures 2(a) and 2(b) by assigning $\alpha_{v,a}$ (= m_v/m_a) a value of 100. From the figure, the following are observed: (1) For the special cases when $\beta_{i,a} = 1$ (i.e., $\omega_a = \omega_i$) and $\beta_{i,a} = \beta_{v,a}$ (i.e., $\omega_v = \omega_i$) (see red dotted lines), the DAF_a tends to a very large value (not infinity), which is defined as the *resonance condition* here. (2) From the resonance regions to the sides, the value of DAF_a gradually decreases, i.e., the amplifier's effect of amplification for the bridge response gradually decreases. Clearly, both equation (23) and Figure 2 can be used to guide the frequency design of the amplifier and vehicle to improve the identifiability of bridge responses.

3.2. Dynamic Amplification Factor of Vehicle for the Bridge Response. Next, the DAF_v is defined as the ratio of the amplitude of each excitation frequency in the *vehicle*

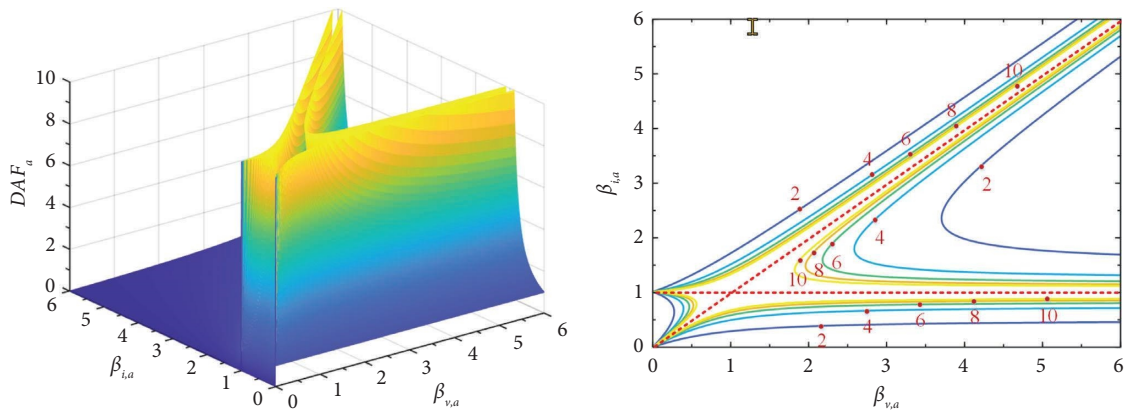

FIGURE 2: DAF_a distribution with respect to $\beta_{v,a}$ and $\beta_{i,a}$: (a) tri-phase; (b) contour.

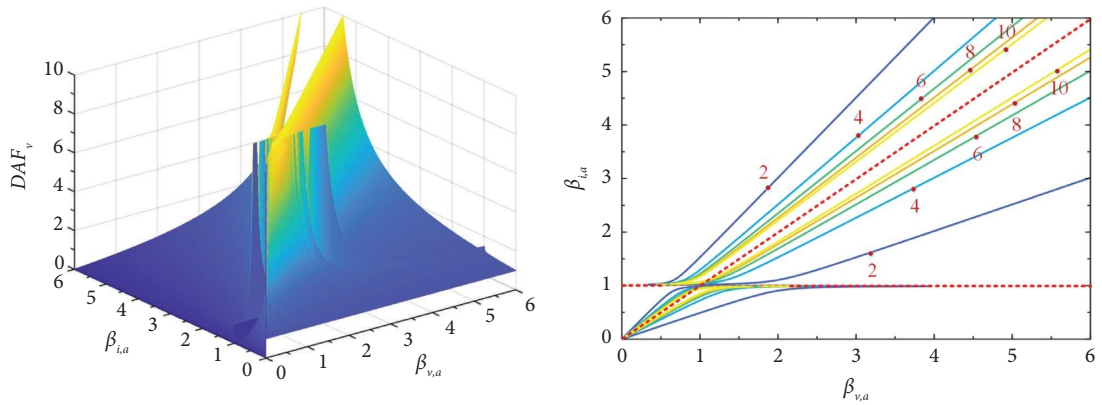

FIGURE 3: DAF_v distribution with respect to $\beta_{v,a}$ and $\beta_{i,a}$: (a) tri-phase; (b) contour.

response to that in the contact response, i.e., the amplitude of each bridge frequency in equation (18) to that in equation (11), namely,

$$\mathrm{DAF}_v\left(\alpha_{v,a},\beta_{v,a},\beta_{i,a}\right)=V_{i,n}=\left|\frac{\alpha_{v,a}\beta_{v,a}\left(\beta_{i,a}-1\right)}{\left(\alpha_{v,a}\beta_{i,a}-\alpha_{v,a}\beta_{v,a}-1\right)\left(\beta_{i,a}-1\right)-1}\right|, \tag{25}$$

meaning that the vehicle's DAF_v is equal to the coefficient $V_{i,n}$ for the frequency i of concern. Also, in deriving the vehicle's DAF_v in equation (25), no assumption was made concerning the smallness of the amplifier mass with respect to the vehicle mass.

By adopting the same value of $\alpha_{v,a}$, i.e., by letting $\alpha_{v,a}=m_v/m_a=100$ as in Figure 2, the curve for the DAF_v with respect to $\beta_{v,a}$ and $\beta_{i,a}$ is plotted in Figure 3. The following were observed: (1) For the special case when $\beta_{i,a}=\beta_{v,a}$ (i.e., $\omega_v=\omega_i$) (see red dotted diagonal), the DAF_v tends to a very large value (not infinity), which is defined as the *resonance* condition, as confirmed by the previous study [50]. (2) For the special case when $\beta_{i,a}=1$ (i.e., $\omega_a=\omega_i$) (see red dotted horizontal line), the DAF_v tends to zero, i.e., the signal transmitted into the vehicle is eliminated, which is defined as the *cancellation* condition to nullify the vehicle response here. It was also under such a (tuned) condition that the "amplifier" has been referred to as *a tuned mass damper* (TMD) in structural engineering. The fact that the DAF_v is equal to the coefficient $V_{i,n}$ is a general expression for the amplification of the input signals (i.e., driving and shifted bridge frequencies) from the contact point to the vehicle.

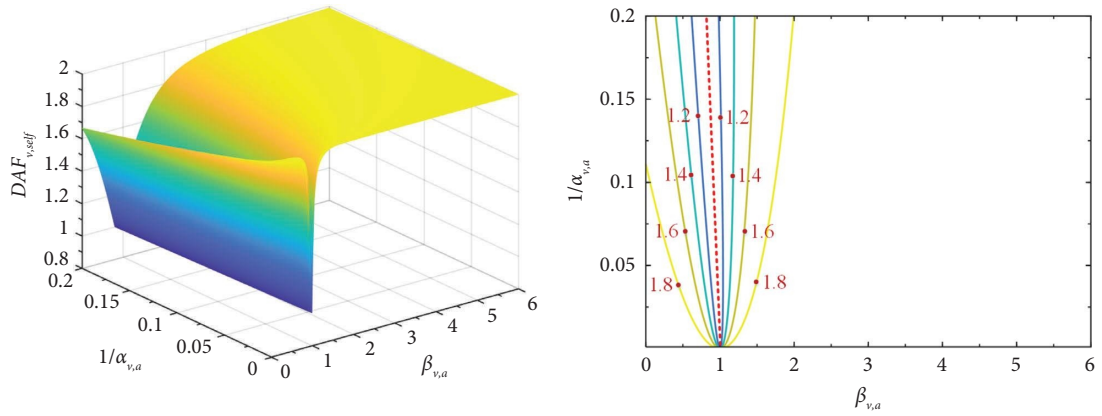

(a) (b)

FIGURE 4: $\mathrm{DAF}_{v,\mathrm{self}}$ distribution with respect to $\beta_{v,a}$ and $1/\alpha_{v,a}$: (a) tri-phase; (b) contour.

3.3. Featured Range of Amplifier Response vs. Vehicle Response. By comparing equation (23) with equation (25), one can obtain the ratio of the amplitude of each excitation frequency in the amplifier response to that in the vehicle response, i.e.,

$$\frac{\mathrm{DAF}_a}{\mathrm{DAF}_v} = \left|\frac{1}{1-\beta_{i,a}}\right|. \tag{26}$$

Evidently, for $0 < \beta_{i,a} < 2$, the value of $\mathrm{DAF}_a/\mathrm{DAF}_v$ in equation (26) is larger than unity, which implies that the frequency amplitude contained in the amplifier response is larger than that in the vehicle response. Thus, the range $0 < \beta_{i,a} < 2$ is regarded as the *featured range* of the amplifier for amplifying the vehicle response.

3.4. Effect of Vehicle Damper on Vehicle's Self-Frequency. In addition to the amplifier's amplification effect on bridge frequencies, one is also interested whether it can assist in suppressing the effect of vehicle's frequency in the vehicle response. In this regard, the amplitude of the vehicle frequency for the n^{th} bridge component is

$$A_v = \begin{cases} \left|\dfrac{\Delta_{st,n}}{2\left(1-S_n^2\right)} V_{1,n}\right|, & \omega_v \geq \omega_a, \\ \left|\dfrac{\Delta_{st,n}}{2\left(1-S_n^2\right)} V_{2,n}\right|, & \omega_v < \omega_a. \end{cases} \tag{27}$$

For the vehicle damper/vehicle mass ratio (m_a/m_v) to be much less than one, equation (27) reduces to

$$A_v = \left|\frac{\Delta_{st,n}}{4\left(1-S_n^2\right)} \widetilde{V} \cdot \mathrm{DAF}_{v,\mathrm{self}}\right|. \tag{28}$$

Here $\mathrm{DAF}_{v,\mathrm{self}}(\alpha_{v,a}, \beta_{v,a})$ is the DAF_v for the vehicle's self-frequency:

$$\mathrm{DAF}_{v,\mathrm{self}}\left(\alpha_{v,a}, \beta_{v,a}\right) = 1 + \left|\frac{-1+\beta_{v,a}+1/\alpha_{v,a}}{\sqrt{\left(1+\beta_{v,a}+1/\alpha_{v,a}\right)^2 - 4\beta_{v,a}}}\right|. \tag{29}$$

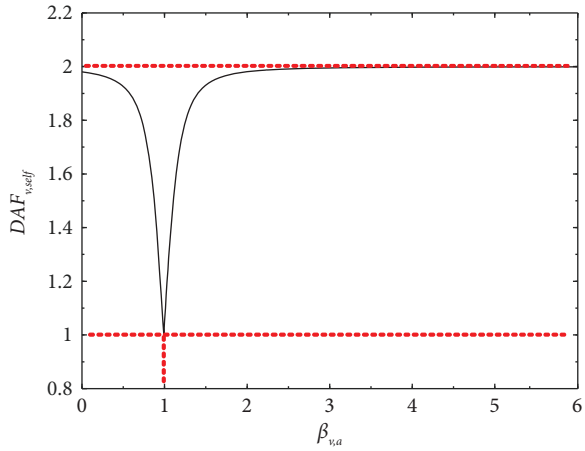

FIGURE 5: Plot of $\mathrm{DAF}_{v,\mathrm{self}}$ with respect to $\beta_{v,a}$ for $\alpha_{v,a}$ =100.

Note that the coefficient $\widetilde{V}$ involved in equation (28) was already given in equation (22), which represents a combination of the components $V_{i,n}$ (with subscript i for (d, n), (bl, n), or (br, n)). Thus, the behavior of the coefficient $\widetilde{V}$ is similar to those for the component $V_{i,n}$ in Section 3.2, which will not be repeated here.

The curve of the $\mathrm{DAF}_{v,\mathrm{self}}$ with respect to the frequency ratio $\beta_{v,a}$ and mass ratio $1/\alpha_{v,a}$ is plotted in Figure 4. It can be observed that when $\beta_{v,a}$ is near 1 (red dotted line), a trough appears in the plot of $DAF_{v,self}$. This can also be explained by equation (29), by noting that for $\beta_{v,a} + 1/\alpha_{v,a} = 1$, the $DAF_{v,self}$ reaches the minimum ($\mathrm{DAF}_{v,\mathrm{self}}$ =1). As stated above, since the vehicle damper mass is very small compared with the vehicle mass, the above condition can be approximated by assuming $\beta_{v,a} + 1/\alpha_{v,a} \cong \beta_{v,a}$ and $\beta_{v,a} = 1$ (i.e., $\omega_a = \omega_v$), as was clearly illustrated in Figure 5 for $\alpha_{v,a} = 100$. In practice, the vehicle damper can generally meet the measurement needs by just setting $\omega_a = \omega_v$, which was also known as the vibration reduction effect of the TMD (now known as the vehicle damper) on the supporting mass (now known as the vehicle). In such a case, the response of the vehicle damper will be greatly amplified. Such

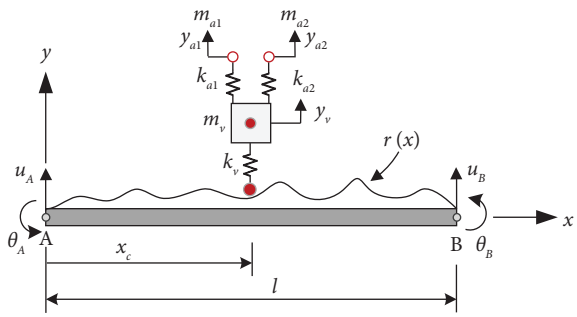

Figure 6: Amplifier-vehicle-bridge interaction element.

a phenomenon will also be verified by numerical simulation in Section 7.

4. Numerical Simulation of the Problem

In this section, the VBI element for the amplifier-vehicle-bridge system will be briefed, which will be used to verify the accuracy and reliability of analytical solutions derived above. Noteworthy is that the finite element analysis is *not* restricted by most of the assumptions adopted in deriving the analytical solutions, such as $(m_v + m_a) \ll mL$.

4.1. Brief of Amplifier-Vehicle-Bridge Interaction Element. To meet the various functions needed in measurement, more than one amplifier may be installed on the test vehicle. In this study, two amplifiers will be installed on the test vehicle to enhance its scanning capability, as shown in Figure 6. Either the test vehicle or each of the two amplifiers will be fitted with an accelerometer to measure the vertical vibration. The bridge is modeled as a beam element, with damping ignored. The vehicle is modeled as a sprung mass m_v supported by a spring of stiffness k_v, and each amplifier is connected to the vehicle body (or axle) by a spring, with amplifier 1 identified as concentrated mass m_{a1} and stiffness k_{a1} and amplifier 2 as concentrated mass m_{a2} and stiffness k_{a2}.The following is the equation of motion for the amplifier-VBI element:

$$\begin{bmatrix} [m_b] & 0 & 0 & 0 \\ 0 & m_v & 0 & 0 \\ 0 & 0 & m_{a1} & 0 \\ 0 & 0 & 0 & m_{a2} \end{bmatrix} \begin{Bmatrix} \{\ddot{u}\} \\ \ddot{y}_v \\ \ddot{y}_{a1} \\ \ddot{y}_{a2} \end{Bmatrix} + \begin{bmatrix} [k_b] + k_v\{N\}_c\{N\}_c^T & -k_v\{N\}_c & 0 & 0 \\ -k_v\{N\}_c^T & k_v + k_{a1} + k_{a2} & -k_{a1} & -k_{a2} \\ 0 & -k_{a1} & k_{a1} & 0 \\ 0 & -k_{a2} & 0 & k_{a2} \end{bmatrix} \begin{Bmatrix} \{u\} \\ y_v \\ y_{a1} \\ y_{a2} \end{Bmatrix} = \begin{Bmatrix} -(k_v r_c + m_{a1} g + m_{a2} g + m_v g)\{N\}_c \\ k_v r_c \\ 0 \\ 0 \end{Bmatrix}, \tag{30}$$

Table 1: Bridge, vehicle, and amplifier properties.

Bridge	Length	$L = 25$ m
	Young's modulus	$E = 27.5$ GPa
	Moment of inertia	$I = 0.15$ m^4
	Mass per unit length	$m = 4{,}800$ kg/m
Vehicle	Mass	$m_v = 1{,}000$ kg
	Stiffness	$k_v = 1{,}500$ kN/m
Amplifier	Mass	$m_a = 10$ kg
	Stiffness	$k_a = 50$ kN/m

where $[m_b]$ and $[k_b]$, respectively, denote the mass and stiffness matrices of the beam element [64]; y_v is the displacement of the vehicle; y_{a1} and y_{a2} are the displacements of the two amplifiers; $\{u\}$ represents the beam displacements; r_c represents the pavement roughness; v represents the vehicle speed; x_c represents the position of the contact point; $\{N\}_c$ represents the cubic Hermitian interpolation function evaluated at x_c. The amplifier-VBI element of equation (30) needs to be assembled with other beam elements that are free of the vehicle to build the global equations of the VBI system. The responses of the VBI system can be solved by the Newmark-β method (with $\beta = 0.25$ and $\gamma = 0.5$ for unconditional stability) [64] via updating of the contact position and global VBI system at each time step.

4.2. Verification of Analytical Solutions. In this section, the reliability of the analytical solutions derived for the bridge, vehicle, and amplifier in Section 2 will be evaluated by the finite element method (FEM) for a typical example. To comply with the analytical solution, only one amplifier is considered by the FEM in this section. The properties of the bridge, vehicle, and amplifier adopted are listed in Table 1, which have been typically used in previous studies to verify the accuracy of the analytical solutions [8, 50, 58]. In the simulation, each element length is taken as $l = 0.5$ m, and the time step is $\Delta t = 0.001$s. The frequencies of the bridge, vehicle, and amplifier calculated by equations (7), (14)–(16), and (16) are listed in Table 2, in terms of the frequency $f = \omega/(2\pi)$. It should be noted that the amplifier and vehicle frequencies calculated by equation (14) (for the coupled amplifier-vehicle system) are very close to the ones calculated by equations (15) and (16) when m_a/m_v is much less than one. For this case, the coupled frequencies will be identified as $\tilde{f}_a$ and $\tilde{f}_v$ for better recognition in Table 2. Identifying each specific frequency of the amplifier-vehicle system is the first issue in application of the VSM. This can be made possible if all the frequencies of the amplifier-vehicle system have been identified in advance by a flat road test [14] or shaking table test, which are free of the bridge properties. Based on this, the frequencies of the bridge can be judged accordingly.

In practice, it is assumed that *both the vehicle and amplifier will be fitted with sensors* for collecting vibration signals. To verify the accuracy of the analytical solutions, pavement roughness is temporarily ignored in this section, i.e., with $r_c = 0$. The analytical (closed-form) solutions will be compared with the FEM results in time and frequency

Table 2: Bridge, vehicle, and amplifier frequencies.

Frequency	Bridge			Vehicle	Amplifier	Coupled amplifier-vehicle system	
	$f_{b,1}$	$f_{b,2}$	$f_{b,3}$	f_v	f_a	$\tilde{f}_v$	$\tilde{f}_a$
Value (Hz)	2.33	9.32	20.97	6.16	11.25	6.12	11.34

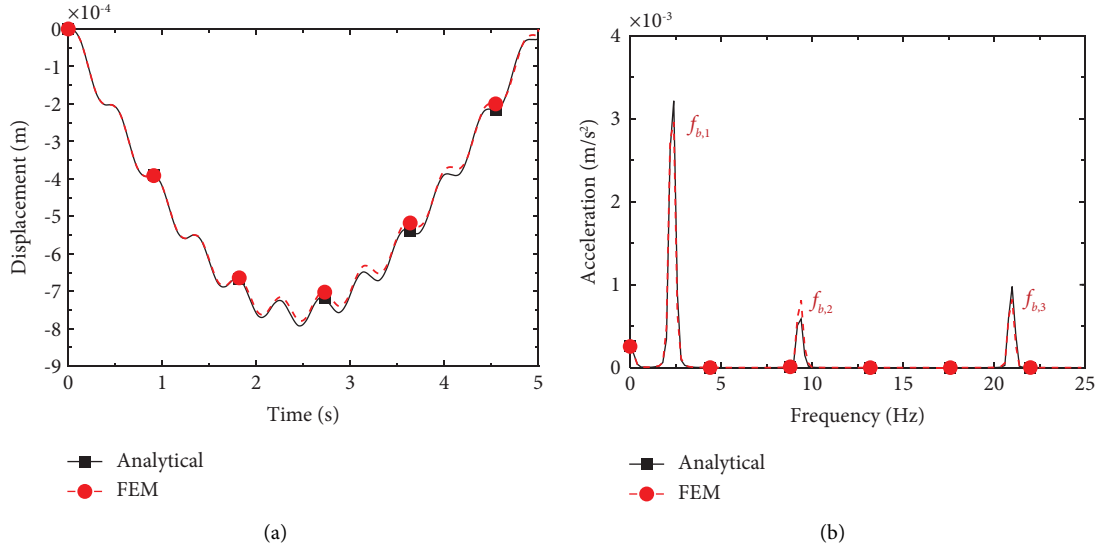

Figure 7: Bridge responses in OB: (a) displacement; (b) acceleration spectrum.

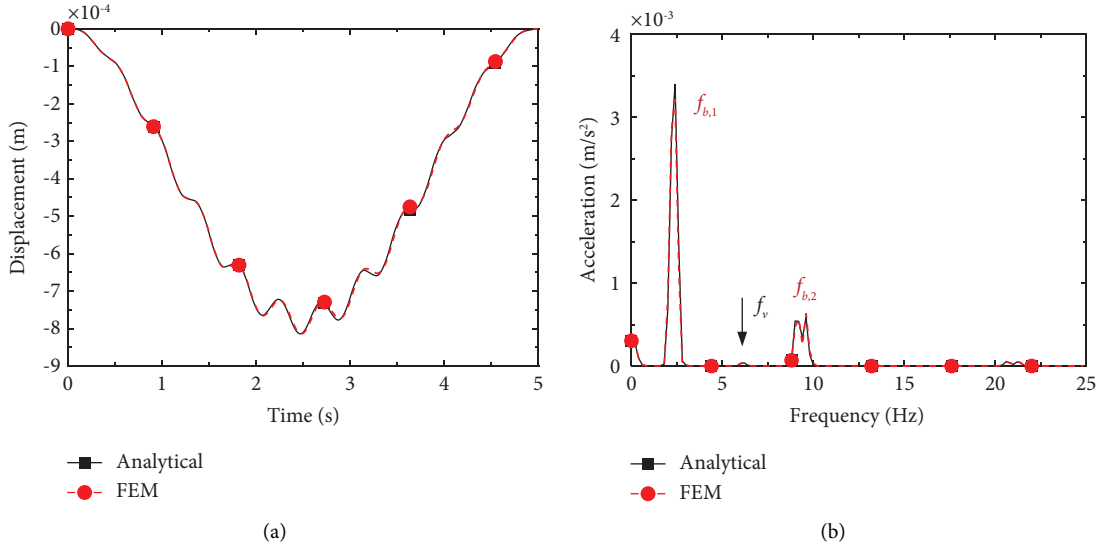

Figure 8: Vehicle responses: (a) displacement; (b) acceleration spectrum.

domains as conventional [8] to validate the irreliability [34, 51, 59]. In fact, this also serves as a benchmark test for the FEM modeling. To tackle a wider range of the problem, only the FEM will be employed, such as the resonance analysis in Section 5 and parametric study in Section 6, since the FEM is not restricted by the assumptions made in deriving the theoretical closed-form solutions. For brevity, only the displacement and acceleration responses of the bridge, vehicle, and amplifier will be presented. To assess the effect of multi-mode contribution, the *observation point* (OB) of the bridge is taken at 11 *m from the left end*, but not at the midspan. For the test vehicle moving at v =5 m/s (18 km/h), the displacements of the bridge's OB calculated analytically and numerically are plotted in Figure 7(a), along

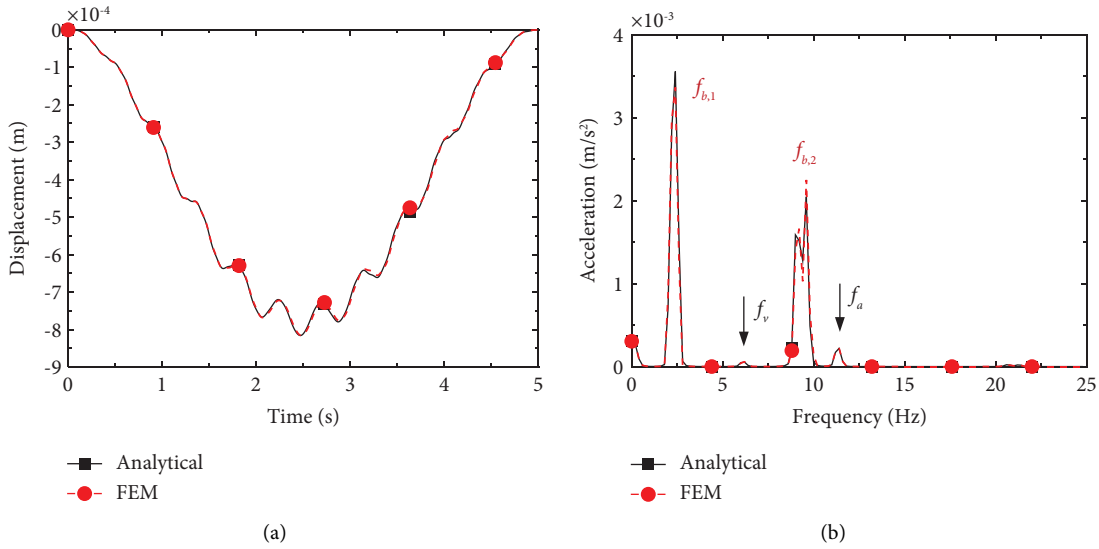

FIGURE 9: Amplifier responses: (a) displacement; (b) acceleration spectrum.

with the acceleration spectra in Figure 7(b). In addition, the displacements and acceleration spectra of the vehicle are plotted in Figures 8(a) and 8(b), respectively, and those of the amplifier in Figures 9(a) and 9(b), for both the analytical and FEM solutions. Evidently, all these figures indicate that the analytical solutions *agree excellently* with the FEM solutions in both time and frequency domains. To facilitate the reading, the frequencies of the amplifier/vehicle have been indicated in black and the frequencies of the bridge (or external excitation frequencies) in red in the figures and throughout the paper.

A comparison of the vehicle spectrum in Figure 8(b) with the amplifier spectrum in Figure 9(b) clearly indicates that the amplifier performs better than the vehicle in that the 2nd bridge frequency $f_{b,2}$ in the amplifier spectrum in Figure 9(b) can be more clearly identified than that in the vehicle spectrum in Figure 8(b), mainly due to the *TMD effect* brought by the proximity of the two frequencies f_a and f_v. This is an illustration of the potential of amplifier in enhancing the identifiability of bridge frequencies, conforming to the statements previously made for Figure 2 and equation (26). (1) When the amplifier frequency is close to the bridge frequency, the amplitude of the bridge frequency in the amplifier response will be amplified (noted as the resonance condition for the amplifier there). (2) For the featured range $0 < \beta_{i,a} < 2$ (the value $\beta_{i,a} = 0.3$ is used here), the amplifier response's performance is better than the vehicle response, as was theoretically shown in Section 3.3.

5. Test Vehicle Set in (or Not in) Resonance

To verify the points of resonance theoretically investigated in Section 3.1, the properties of the amplifier and test vehicle remain identical to those used in Section 5. Particularly, the amplifier frequency is $f_a = 11.25\,Hz$ and the vehicle frequency is $f_v = 6.16\,Hz$. Consider a harmonic excitation, $u_c(t) = \sin(2\pi f_{\text{inp}} t)$, on the amplifier-vehicle system in Figure 10, for two different excitation frequencies: Case 1

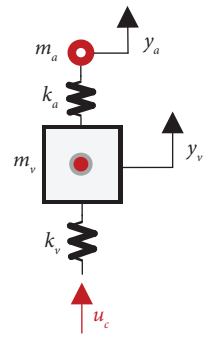

FIGURE 10: Amplifier-vehicle system.

(test vehicle set in resonance): $f_{\text{inp}} = f_v = 6.16\,Hz$, which is near $\widetilde{f}_v = 6.12\,Hz$ (coupled); Case 2 (test vehicle set not in resonance): $f_{\text{inp}} = f_a = 11.25\,Hz$, which is near $\widetilde{f}_a = 11.34\,Hz$ (coupled). The accelerations of the input excitation, amplifier, and vehicle are plotted in Figure 11(a) for Case 1, together with the spectra in Figure 11(b), and the ones for Case 2 are plotted in Figure 12.

For Case 1 (test vehicle set in resonance) in Figure 11, the excitation frequencies f_{inp} in both the vehicle and amplifier responses have been violently amplified, mainly due to resonance on the test vehicle [50], and the vibration was strongly amplified and transmitted to the amplifier.

For Case 2, the test vehicle was not set in resonance, but the amplifier was set in the *tuned* or *cancellation* condition (with $f_{\text{inp}} = f_a$) to nullify the vehicle response, as theoretically analyzed in Sections 3.1 and 3.2. As can be seen from Figure 12, the excitation frequency f_{inp} in the amplifier response has been drastically amplified as expected. In contrast, the excitation frequency f_{inp} is rather small in the vehicle response, mainly due to the *TMD effect* of the amplifier, once the cancellation condition is met by the amplifier. In practice, when applying the VSM to bridges, due to the shifting effect of the moving speed, the bridge

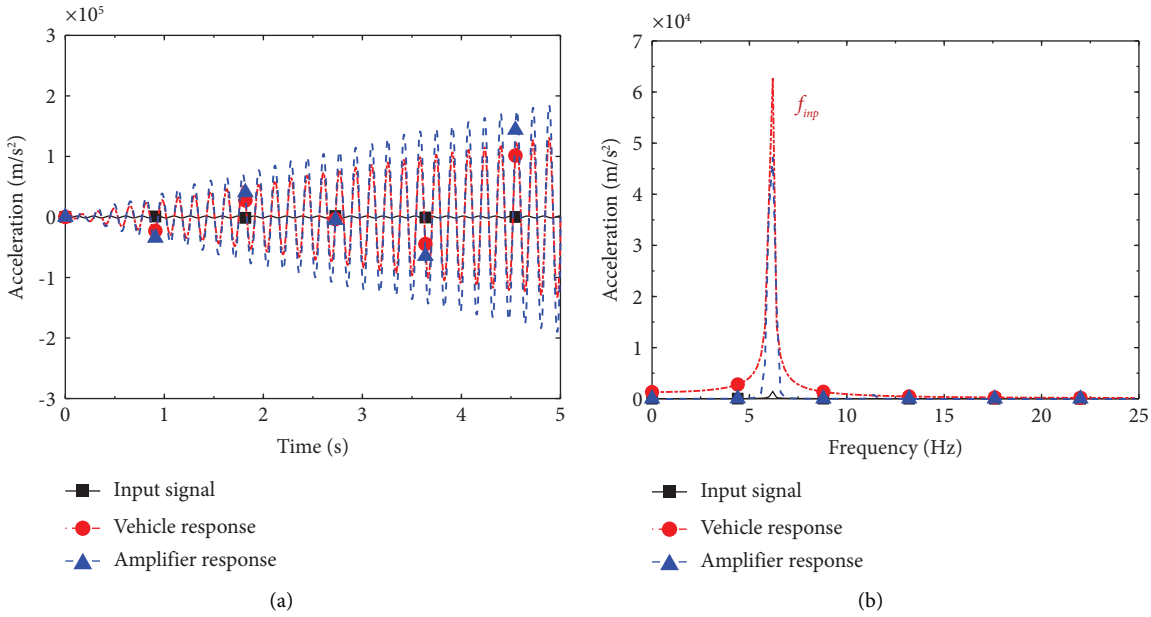

Figure 11: Acceleration responses of Case 1: (a) acceleration; (b) acceleration spectrum.

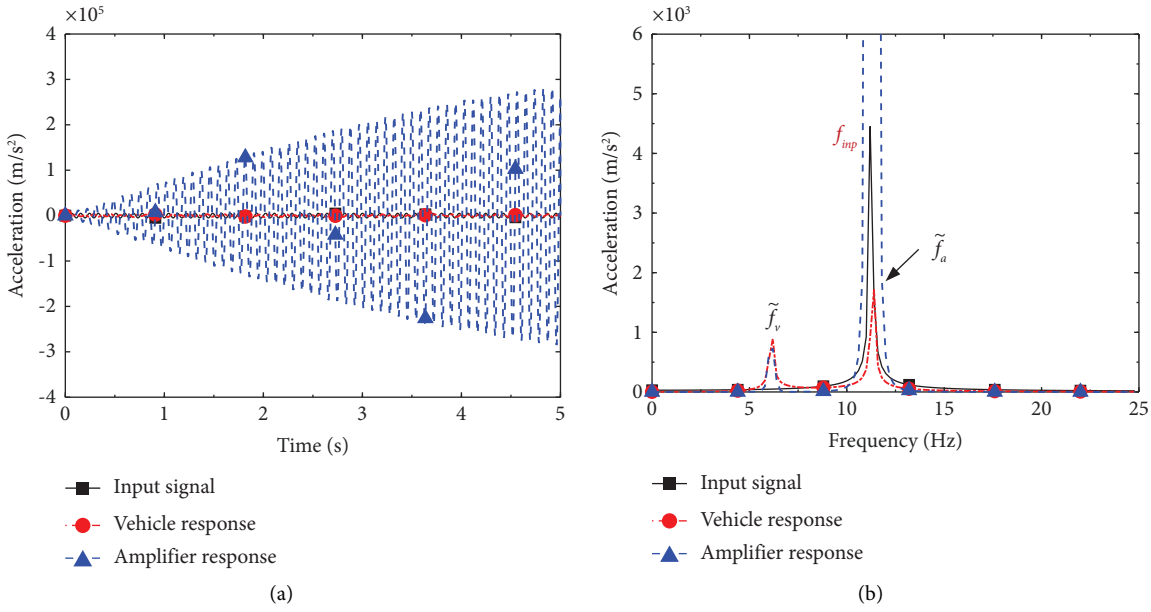

Figure 12: Acceleration responses of Case 2: (a) acceleration; (b) acceleration spectrum.

frequency $f_{b,n}$ in the vehicle response was divided into two frequencies $f_{bl,n}$ and $f_{br,n}$, which explains why the bridge frequency is still present in the vehicle responses under the cancellation condition.

6. Effect of Amplifier on Bridge Frequency Extraction

To assess the amplification effect of the amplifier in extraction of bridge frequencies, the frequency and mass of the amplifier will be studied. In addition, to demonstrate the advantage of using the amplifier for bridge frequency identification, both the vehicle and amplifier responses generated by the FEM will be compared. The properties adopted of the bridge and vehicle are the same as those used in Section 4, unless noted otherwise. The stiffness and mass of the amplifier can be adjusted to meet the measurement needs.

6.1. Effect of Amplifier Mass. Generally, the amplifier mass is very small compared with the vehicle mass. To focus on the effect of amplifier mass on bridge frequency extraction, the amplifier frequency is first kept unchanged, i.e., with $f_a = 11.25$ Hz, as listed in Table 2. Four masses are

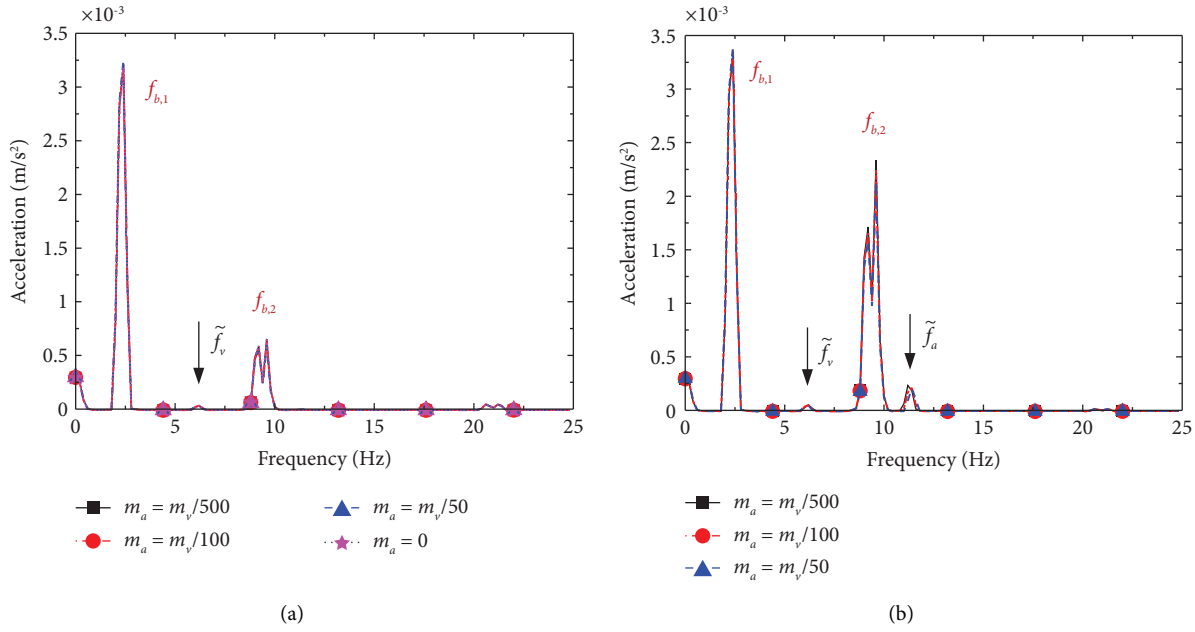

Figure 13: Acceleration responses of the amplifier-vehicle system for different mass ratios: (a) vehicle; (b) amplifier.

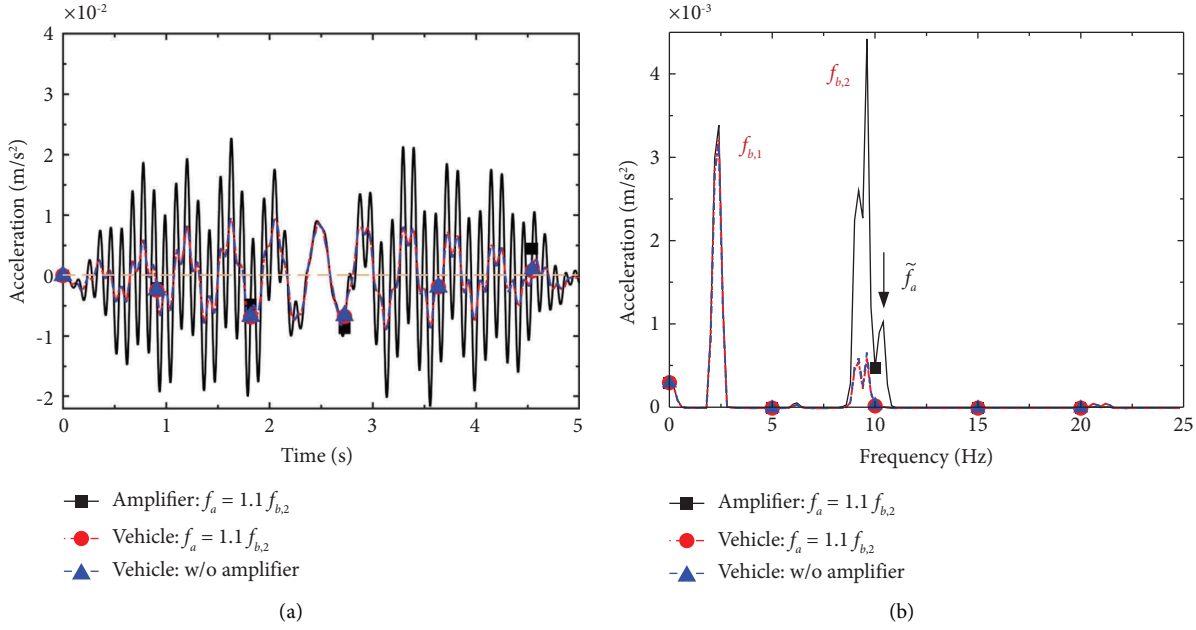

Figure 14: Acceleration responses of the amplifier-vehicle system for $f_a = 1.1\ f_{b,2}$: (a) acceleration; (b) acceleration spectrum.

considered for the amplifier m_a: $m_v/500, m_v/100, m_v/50$, and 0 (reference only). Correspondingly, the stiffness of the amplifier is adjusted as $k_a = 10, 50$, and 100 kN/m for the three masses, respectively. The vehicle and amplifier responses calculated are plotted in Figures 13(a) and 13(b), respectively. As can be seen, the effect of amplifier mass has resulted in *little changes* in the amplitudes of bridge frequencies in both vehicle and amplifier responses for all the cases, aside from the fact that the amplifier performs better than the vehicle, particularly for the 2nd bridge frequency. This confirms that the amplifier mass can be neglected in practice.

6.2. Effect of Amplifier Frequency. Bridge frequencies are the quantities to be measured, but they are unknown prior to measurement. However, to demonstrate the capability of the amplifier presented in Section 3.1, the frequency of amplifier is set to 1.1 times the bridge frequency, i.e., $f_a = 1.1\ f_{b,n}$, aimed at amplifying the bridge frequency of concern, while

avoiding the resonance condition mentioned in Section 3.1. In the measurement, the amplifier can be tuned by the forward and backward trips. In the forward trip, the bridge frequencies can be measured from the test vehicle response, though a small amplitude. Then, the amplifier frequency can be tuned in the backward trip to better identify the bridge frequencies. The mass of the amplifier used in this section is identical to that in Section 4.

Firstly, the amplifier is tuned to a frequency close to the 2nd bridge frequency, i.e., $f_a = 1.1\, f_{b,2}$ (by adjusting the amplifier stiffness as $k_a = 41.49\, kN/m$). The acceleration responses of the vehicle and amplifier computed by the FEM are plotted in Figures 14(a) and 14(b). As can be seen, the vehicle *responses* obtained for the two cases, i.e., with and without amplifier, are almost the same, meaning that the vehicle response is virtually not affected by the presence of the amplifier (relatively small). However, from Figure 14(b), one observes that the *2nd bridge frequency* has been significantly amplified in the amplifier response, compared with that in the vehicle response, indicating that the amplifier is a better device than the vehicle for bridge frequency extraction.

Next, the amplifier is tuned to a frequency close to the 3rd bridge frequency, i.e., $f_a = 1.1\, f_{b,3}$ (by adjusting the amplifier stiffness as $k_a = 210.04\, kN/m$). The acceleration responses of the vehicle and amplifier obtained by the FEM are plotted in Figure 15. Again, the 3rd bridge frequency in the amplifier response has been made more visible than that in the vehicle response. For the above two cases, the value of $\beta_{i,a}(\beta_{i,a} = f_{b,n}^2/f_a^2 = 0.826)$ remains unchanged, and the value of $\beta_{v,a}$ $(\beta_{v,a} = f_v^2/f_a^2)$ decreases as f_a increases. As can be seen from Figure 2(b), the DAF_a decreases as $\beta_{v,a}$ decreases for $\beta_{i,a} = f_{b,n}^2/f_a^2 = 0.826$ and $\beta_{v,a} = f_v^2/f_a^2 < 1$ (for the present two cases). Therefore, the amplification effect on the 3rd bridge frequency is reduced. Nevertheless, the bridge amplifier can still make certain contribution to identification of the 3rd bridge frequency. The above investigation indicates that *the amplifier can be adopted to improve the identifiability of bridge frequencies* via *tuning* of the amplifier frequency. In [58], it was demonstrated that the frequency of the amplifier can be easily adjusted, the so-called *adaptive amplifier*, by attaching the amplifier (accelerometer) to a cantilever that is rigidly connected to the vehicle body (or axle). Such a device enables the frequency of the amplifier to be easily tuned by adjustment of the arm length of the cantilever.

6.3. Dual Amplifiers for the Bridge Frequencies. In this section, two amplifiers will be mounted on the test vehicle each to amplify the 2nd and 3rd frequencies of the bridge. That is, amplifier 1 is tuned to a frequency close to the 2nd bridge frequency, i.e., $f_{a1} = 1.1\, f_{b,2}$, and amplifier 2 to a frequency close to the 3rd bridge frequency, i.e., $f_{a2} = 1.1\, f_{b,3}$.

The acceleration responses of the vehicle and two amplifiers computed by the FEM are plotted in Figure 16. As can be seen, the 2nd bridge frequency has been significantly amplified in response of amplifier 1. Also, some amplification effect has been achieved for the 3rd bridge frequency in response of amplifier 2, compared with the original vehicle response. However, the level of amplification is not comparable to that for amplifier 1. From this study, one learns that *the amplifier can offer some magnification effect on the bridge frequency, but the effectiveness decreases as the order of frequency increases*. Theoretically, any of the bridge frequencies can be magnified via installation of the amplifier, but there is a limit on the effectiveness.

7. Effect of Pavement Roughness

Pavement roughness is known to affect the effectiveness of the VSM in that it may exaggerate the vehicle frequency in the vehicle's spectrum such that the bridge frequencies desired are overshadowed [14]. In this regard, two functions will be investigated for the amplifier concerning (1) suppression of the effect of vehicle's frequency by tuning its frequency to the vehicle frequency and (2) amplification of bridge's frequencies in the presence of pavement roughness. The pavement roughness is generated by the power spectral density (PSD) function of ISO 8608 with class A [65], shown as the black curve in Figure 17. Currently, there is no specification set for bridge pavement roughness. According to our previous field experience, the pavement of bridges is generally in a better condition than that of the roads as implied by ISO 8608, due to the fact that the former receives more care from bridge administrators and maintenance engineers. In addition, the real contact between the pavement and vehicle's wheels is a "circular surface" rather than a "point" [66]. Based on the above reasons, the original roughness profile has been smoothed (i.e., with the acute extrema reduced) by the moving average filter (MAF) [67], shown as the red curve in Figure 17.

7.1. Vehicle Damper Frequency Tuned to Vehicle Frequency. It was known that the vehicle's self-frequency in the vehicle response will overshadow the bridge frequencies. As was theoretically shown in Section 3.4, the $\mathrm{DAF}_{v,\mathrm{self}}$ for vehicle's self-frequency will reach the minimum for $\beta_{v,a}$ near 1 (i.e., for $\omega_a = \omega_v$). When the vehicle damper is tuned to the frequency of the test vehicle, it acts as a TMD for reducing the amplitude of vehicle's frequency. The TMD has been widely used in vibration control of buildings and bridges, of which the optimal parameters were investigated in previous studies [68–71]. However, the TMD was rarely applied to the VSM to enhance the performance of the test vehicle. To investigate such a suppression effect on vehicle's self-frequency, the vehicle damper frequency is tuned to the vehicle frequency, i.e., with $f_a = f_v = 6.16\, Hz$, as listed in Table 2. Four masses are considered for the vehicle damper mass m_a: $m_v/500, m_v/100, m_v/50$, and 0 (reference only). Accordingly, the stiffness of the vehicle damper is adjusted as $k_a = 3, 15$, and $30\, kN/m$ for the three masses, respectively. For the four cases, the acceleration of the vehicle moving over the bridge with rough surface has been calculated by the FEM and is plotted in Figure 18(a), along with the corresponding spectra in Figure 18(b). The first impression of Figure 18(b) is that the vehicle damper mass tends to reduce the amplitude of the vehicle frequency as was theoretically shown

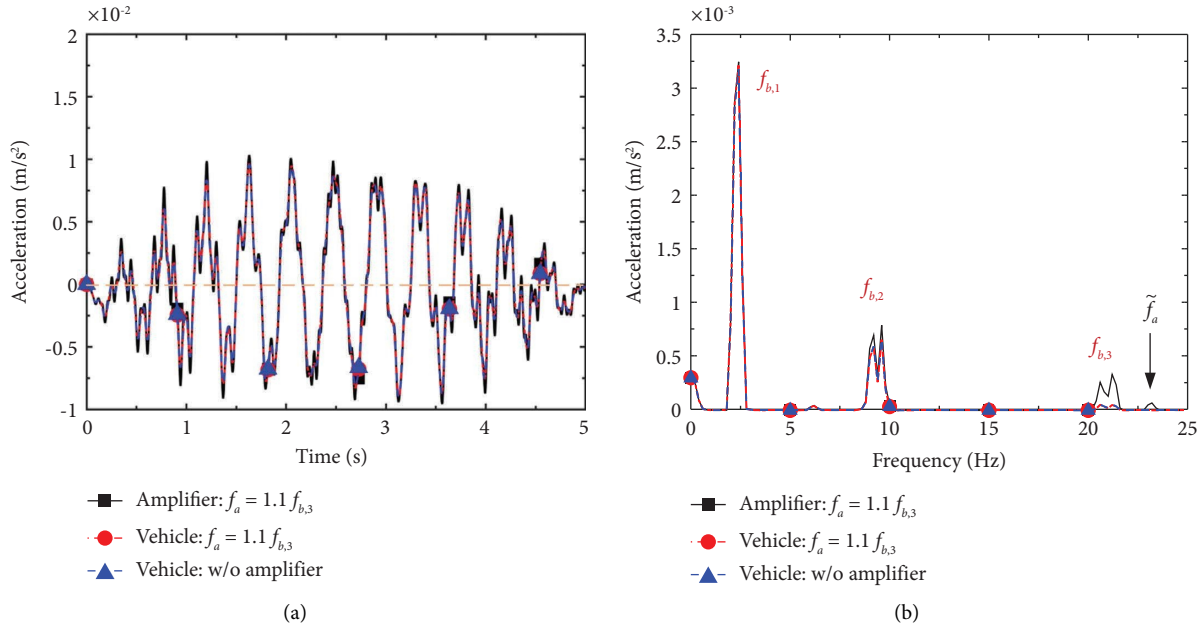

Figure 15: Acceleration responses of the amplifier-vehicle system for $f_a = 1.1\ f_{b,3}$: (a) acceleration; (b) acceleration spectrum.

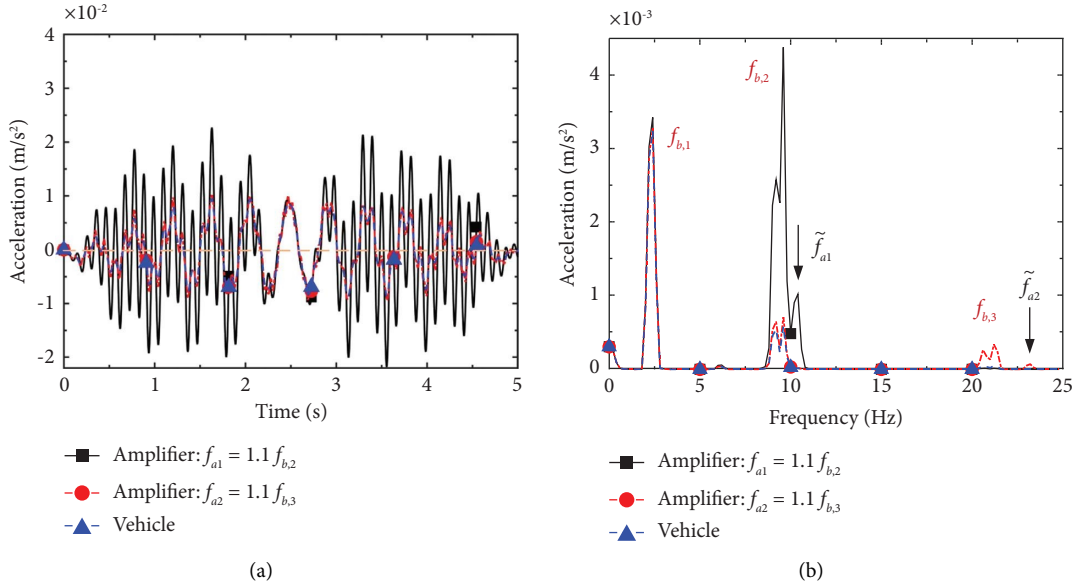

Figure 16: Acceleration responses of the vehicle and two amplifiers: (a) acceleration; (b) acceleration spectrum.

in Section 3.4, and the suppression effect becomes more obvious as the vehicle damper mass m_a increases from $m_v/500$ to $m_v/50$. In short, *for $f_a = f_v$, a larger vehicle damper mass has a better suppression effect on the vehicle frequency.*

7.2. Dual Amplifiers Tuned for Different Functions. In this section, two amplifiers will be mounted on the test vehicle, the bridge amplifier is tuned to a bridge frequency (for amplification) [58], and the vehicle damper is tuned to the vehicle's self-frequency, to serve as a *TMD for the vehicle*, as was investigated in Section 7.1. The bridge amplifier is tuned to a frequency close to the 2nd bridge frequency (i.e., $f_a = 11.25\,Hz$ and $m_a = m_v/100$, which are identical to those in Section 4.2), and the vehicle damper is tuned to the vehicle frequency (i.e., $f_{\mathrm{TMD}} = f_v = 6.16\,Hz$ and $m_{\mathrm{TMD}} = m_v/50$, which are identical to those of the 3rd case in Section 7.1).

A health monitoring method that does not hinder the operation of traffic is essential to the normal functioning of the local society. One advantage with application of the VSM is that ongoing traffic on the bridge need not be terminated during the test. In fact, ongoing traffic can "pump" more vibration energy into the bridge and enlarge the modal

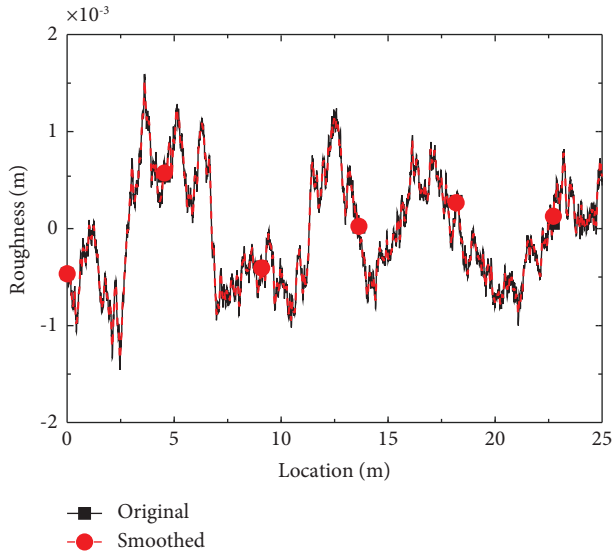

Figure 17: Road roughness.

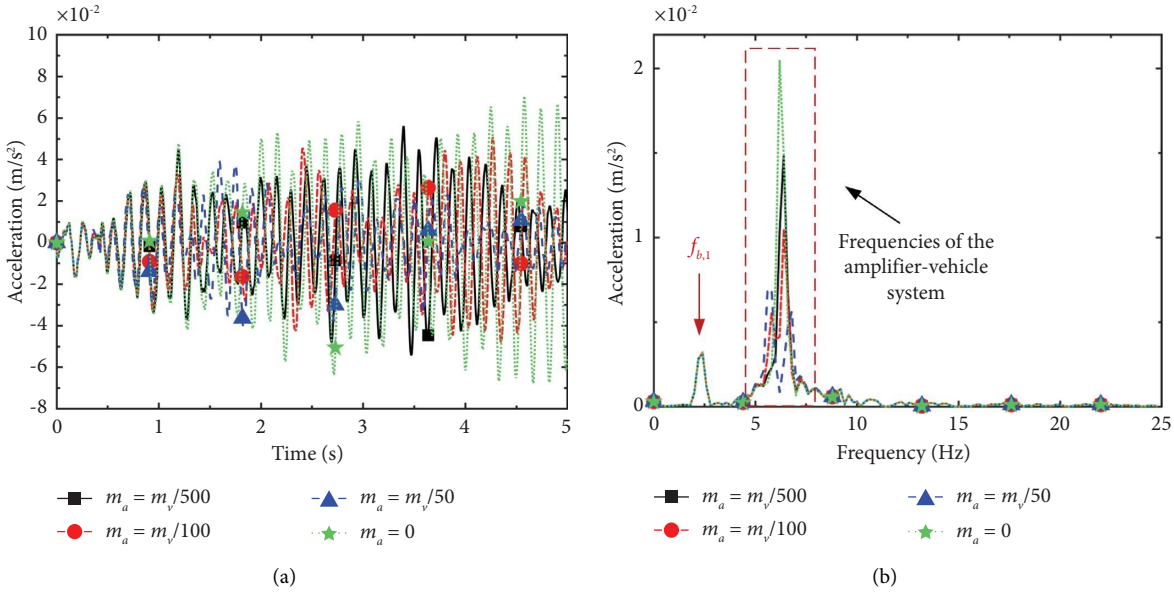

Figure 18: Acceleration responses of the vehicle for $\beta_{v,a} = 1$: (a) acceleration; (b) acceleration spectrum.

Table 3: Traffic flow data.

Traffic flow	Car 1	Car 2	Car 3	Car 4
Entry time (s)	−0.11	1.36	−0.45	2.13
Speed (km/h)	41	37	49	46
Mass (kg)	1,277	1,405	1,656	1,549

responses of the bridge for easy identification. Previously, ongoing traffic has been often employed to outbalance the "negative" pollution effect brought by surface roughness. For the present purposes, four additional vehicles of different (concentrated) masses and speeds with different entry times onto the bridge generated by a random software program are adopted, as listed in Table 3. The test vehicle's entry time is 0 s. In addition, Cars 1 and 2 enter into the bridge from the same end as the test vehicle, but Cars 3 and 4 from the other end.

It should be admitted that the bridge mass used in Table 1 is assumed for a "one-lane bridge" merely to show the idea of the method proposed herein. In practice, a road bridge contains multiple lanes, and the mass of the bridge is many times larger, which means that the mass ratio of the vehicles (test vehicle and traffic flow) to the bridge is much smaller in the real world than the case assumed. Besides, the speeds of the traffic flow in Table 3 are much faster than those of the test vehicle. The most severe duration for all vehicles to stay on the bridge is only 0.37 s, which is quite short compared with the travel time of the test vehicle. Also,

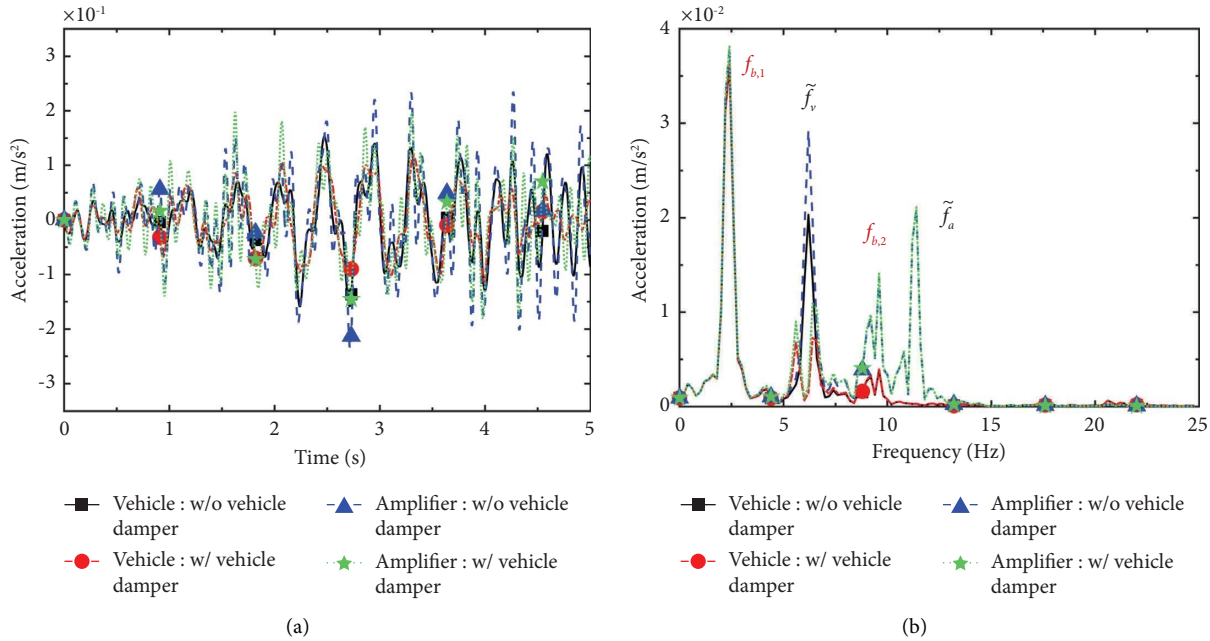

Figure 19: Acceleration responses of the vehicle and amplifier: (a) acceleration; (b) acceleration spectrum.

the maximum vehicles/bridge mass ratio encountered in the simulation is 0.044, when four vehicles (test vehicle and Cars 1–3) are traveling simultaneously on the bridge. According to [72], the bridge frequencies will remain almost unaffected by the test vehicle and ongoing traffic.

The accelerations and spectra of the vehicle and bridge amplifier with the aid of the vehicle damper are plotted in Figures 19(a) and 19(b), respectively, along with the case with no vehicle damper for reference. As can be seen from Figure 19(b), only the 1st bridge frequency $f_{b,1}$ can be clearly identified in the spectra of the vehicle with no vehicle damper. But from the amplifier spectra, whether with or without vehicle damper, the first two bridge frequencies $f_{b,1}$ and $f_{b,2}$ can be identified. In addition, it can be found that with the aid of the vehicle damper, the amplitudes of the vehicle frequency in both the vehicle and amplifier responses are significantly suppressed. Overall, the bridge amplifier with the aid of the vehicle damper performs the best in bridge frequency scanning in that *two bridge frequencies can be identified by the bridge amplifier even in the presence of pavement roughness*, and that the vehicle frequency's effect has been virtually suppressed by the vehicle damper, as desired.

8. Concluding Remarks

In this theoretical study, dual-function amplifiers are proposed for enhancing the capability of a scanning test vehicle for bridges. Firstly, closed-form solutions for the dynamic responses of the amplifier-vehicle-bridge system with a moving test vehicle are presented. Next, the dynamic amplification factors of the amplifier and vehicle are derived for investigating the transmissibility of the response from the bridge to the vehicle and amplifier. To tackle the two main obstacles with the vehicle scanning method, dual amplifiers are proposed as an addition to the test vehicle, with one (i.e., vehicle damper) used to suppress the effect of vehicle's frequency and the other (i.e., bridge amplifier) to amplify the bridge frequency of concern. The feasibility of the proposed method was verified numerically for the key parameters involved. Based on the theoretical and numerical studies presented herein, the following conclusions are drawn:

(1) The amplifier can be adopted to improve the identifiability of bridge frequencies via tuning of its frequency to the bridge frequency of interest.

(2) The amplifier performs better than the vehicle in extraction of bridge frequencies in the range of $0 < \beta_{i,a}\,(\omega_i^2/\omega_a^2) < 2$, which is called the featured range of the amplifier.

(3) Amplifier mass results in very slight changes in the amplitudes of bridge frequencies in both the vehicle and amplifier responses, which can be neglected in practice.

(4) By tuning the vehicle damper's frequency to the vehicle's self-frequency, the vehicle damper becomes a TMD of the vehicle. Under such a condition, the vehicle's response will be suppressed, while the vehicle damper's response will be amplified.

(5) The proposed dual-function amplifier system as an addition to the moving test vehicle has been demonstrated to be effective for scanning the first two bridge frequencies, even in the presence of rough pavements.

As an ending remark, it is admitted that all the bridge frequencies are unknown prior to the measurement. However, if a pretest can be conducted by allowing the test vehicle to travel the bridge for two to three times, then an estimate can be made for the range of the first few bridge

frequencies, which can then be targeted and tuned using the dual amplifiers proposed herein. In addition, this study is aimed at the formation of the theoretical framework for the dual amplifiers to enhance the function of a scanning vehicle for bridges. The theoretical framework presented herein will be extended to experimental and field studies in the future study.

Data Availability

The data used to support the findings of this study are available from the corresponding authors upon reasonable request.

Conflicts of Interest

The authors declare that they have no conflicts of interest.

Authors' Contributions

H. Xu was responsible for conceptualization, methodology, formal analysis, software, funding acquisition, and writing/editing, and writing/editing the original draft. M. Yang contributed to data curation and performed formal analysis. J.P. Yang was responsible for methodology, formal analysis, software, funding acquisition, and proofreading. Z.L. Wang was responsible for formal analysis and software. K. Shi performed software validation. Y.B. Yang conceptualized and supervised the study, was responsible for funding acquisition, and reviewed and edited the paper.

Acknowledgments

This research was supported by National Natural Science Foundation of China (grant nos. 52208146 and 52078082), Chongqing Science and Technology Commission (grant nos. CSTB2022NSCQ-MSX1471, 2022YSZX-JSX0004CSTB, and cstc2021yszx-jscxX0001), China Postdoctoral Science Foundation (grant no. 2022M720580), and National Science and Technology Council, Taiwan (MOST-111-2628-E-A49-009-MY3).

References

[1] Y. J. Yan, L. Cheng, Z. Y. Wu, and L. H. Yam, "Development in vibration-based structural damage detection technique," *Mechanical Systems and Signal Processing*, vol. 21, no. 5, pp. 2198–2211, 2007.

[2] W. Fan and P. Z. Qiao, "Vibration-based damage identification methods: a review and comparative study," *Structural Health Monitoring*, vol. 10, no. 1, pp. 83–111, 2011.

[3] J. Li, S. S. Law, and H. Hao, "Improved damage identification in bridge structures subject to moving loads: numerical and experimental studies," *International Journal of Mechanical Sciences*, vol. 74, pp. 99–111, 2013.

[4] B. Li, S. Wang, X. Wu, and B. Wang, "Dynamic response of continuous beams with discrete viscoelastic supports under sinusoidal loading," *International Journal of Mechanical Sciences*, vol. 86, pp. 76–82, 2014.

[5] R. R. Hou and Y. Xia, "Review on the new development of vibration-based damage identification for civil engineering structures: 2010-2019," *Journal of Sound and Vibration*, vol. 491, Article ID 115741, 2021.

[6] S. Y. Zhang, X. Sheng, J. Z. Jiang, H. Zhou, W. X. Ren, and Z. H. Zhang, "Vibration suppression of bridges under moving loads using the structure-immittance approach," *International Journal of Mechanical Sciences*, vol. 211, Article ID 106792, 2021.

[7] M. Zhang, F. Xu, and H. Yu, "A simplified model to evaluate peak amplitude for vertical vortex-induced vibration of bridge decks," *International Journal of Mechanical Sciences*, vol. 192, Article ID 106145, 2021.

[8] Y. B. Yang, C. W. Lin, and J. D. Yau, "Extracting bridge frequencies from the dynamic response of a passing vehicle," *Journal of Sound and Vibration*, vol. 272, no. 3-5, pp. 471–493, 2004.

[9] C. W. Lin and Y. B. Yang, "Use of a passing vehicle to scan the fundamental bridge frequencies: an experimental verification," *Engineering Structures*, vol. 27, no. 13, pp. 1865–1878, 2005.

[10] P. J. McGetrick, A. González, and E. J. Obrien, "Theoretical investigation of the use of a moving vehicle to identify bridge dynamic parameters," *Insight - Non-Destructive Testing and Condition Monitoring*, vol. 51, no. 8, pp. 433–438, 2009.

[11] D. M. Siringoringo and Y. Fujino, "Estimating bridge fundamental frequency from vibration response of instrumented passing vehicle: analytical and experimental study," *Advances in Structural Engineering*, vol. 15, no. 3, pp. 417–433, 2012.

[12] X. Kong, C. S. Cai, and B. Kong, "Numerically extracting bridge modal properties from dynamic responses of moving vehicle," *J Eng Mech-ASCE*, vol. 142, no. 6, Article ID 04016025, 2016.

[13] S. Urushadze and J. D. Yau, "Experimental verification of indirect bridge frequency measurement using a passing vehicle," *Procedia Engineering*, vol. 190, pp. 554–559, 2017.

[14] Y. B. Yang, H. Xu, B. Zhang, F. Xiong, and Z. L. Wang, "Measuring bridge frequencies by a test vehicle in non-moving and moving states," *Engineering Structures*, vol. 203, Article ID 109859, 2020.

[15] Y. B. Yang, Y. C. Li, and K. C. Chang, "Constructing the mode shapes of a bridge from a passing vehicle: a theoretical study," *Smart Structures and Systems*, vol. 13, no. 5, pp. 797–819, 2014.

[16] A. Malekjafarian and E. J. Obrien, "Identification of bridge mode shapes using short time frequency domain decomposition of the responses measured in a passing vehicle," *Engineering Structures*, vol. 81, pp. 386–397, 2014.

[17] Z. Q. Qi and F. T. K. Au, "Identifying mode shapes of girder bridges using dynamic responses extracted from a moving vehicle under impact excitation," *International Journal of Structural Stability and Dynamics*, vol. 17, no. 08, Article ID 1750081, 2017.

[18] W. Y. He, W. X. Ren, and X. H. Zuo, "Mass-normalized mode shape identification method for bridge structures using parking vehicle-induced frequency change," *Structural Control and Health Monitoring*, vol. 25, no. 6, p. e2174, 2018.

[19] J. Li, X. Q. Zhu, S. S. Law, and B. Samali, "Indirect bridge modal parameters identification with one stationary and one moving sensors and stochastic subspace identification," *Journal of Sound and Vibration*, vol. 446, pp. 1–21, 2019.

[20] Y. Zhang, H. S. Zhao, and S. T. Lie, "Estimation of mode shapes of beam-like structures by a moving lumped mass," *Engineering Structures*, vol. 180, pp. 654–668, 2019.

[21] C. Tan, N. Uddin, E. J. Obrien, P. J. McGetrick, and C. W. Kim, "Extraction of bridge modal parameters using

passing vehicle response," *Journal of Bridge Engineering*, vol. 24, no. 9, Article ID 04019087, 2019.

[22] S. Sadeghi Eshkevari, T. J. Matarazzo, and S. N. Pakzad, "Bridge modal identification using acceleration measurements within moving vehicles," *Mechanical Systems and Signal Processing*, vol. 141, Article ID 106733, 2020.

[23] S. S. Eshkevari, S. N. Pakzad, M. Takác, and T. J. Matarazzo, "Modal identification of bridges using mobile sensors with sparse vibration data," *J Eng Mech-ASCE*, vol. 146, no. 4, Article ID 04020011, 2020.

[24] X. Jian, Y. Xia, and L. Sun, "An indirect method for bridge mode shapes identification based on wavelet analysis," *Structural Control and Health Monitoring*, vol. 27, no. 12, Article ID e2630, 2020.

[25] Q. Mei, N. Shirzad-Ghaleroudkhani, M. Gül, S. F. Ghahari, and E. Taciroglu, "Bridge mode shape identification using moving vehicles at traffic speeds through non-parametric sparse matrix completion," *Structural Control and Health Monitoring*, vol. 28, no. 7, Article ID e2747, 2021.

[26] D. S. Yang and C. M. Wang, "Modal properties identification of damped bridge using improved vehicle scanning method," *Engineering Structures*, vol. 256, Article ID 114060, 2022.

[27] Y. B. Yang, H. Xu, Z. L. Wang, and K. Shi, "Using vehicle-bridge contact spectra and residue to scan bridge's modal properties with vehicle frequencies and road roughness eliminated," *Structural Control and Health Monitoring*, vol. 29, no. 8, Article ID E2968, 2022.

[28] H. Xu, Y. H. Liu, M. Yang, D. S. Yang, and Y. B. Yang, "Mode shape construction for bridges from contact responses of a two-axle test vehicle by wavelet transform," *Mechanical Systems and Signal Processing*, vol. 195, Article ID 110304, 2023.

[29] A. González, E. J. Obrien, and P. J. McGetrick, "Identification of damping in a bridge using a moving instrumented vehicle," *Journal of Sound and Vibration*, vol. 331, no. 18, pp. 4115–4131, 2012.

[30] J. Keenahan, E. J. Obrien, P. J. McGetrick, and A. Gonzalez, "The use of a dynamic truck–trailer drive-by system to monitor bridge damping," *Structural Health Monitoring*, vol. 13, no. 2, pp. 143–157, 2013.

[31] J. Q. Bu, S. S. Law, and X. Q. Zhu, "Innovative bridge condition assessment from dynamic response of a passing vehicle," *Journal of Engineering Mechanics*, vol. 132, no. 12, pp. 1372–1379, 2006.

[32] K. V. Nguyen and H. T. Tran, "Multi-cracks detection of a beam-like structure based on theon-vehicle vibration signal and wavelet analysis," *Journal of Sound and Vibration*, vol. 329, no. 21, pp. 4455–4465, 2010.

[33] Y. Zhang, S. T. Lie, and Z. Xiang, "Damage detection method based on operating deflection shape curvature extracted from dynamic response of a passing vehicle," *Mechanical Systems and Signal Processing*, vol. 35, no. 1-2, pp. 238–254, 2013.

[34] B. Zhang, Y. Qian, Y. T. Wu, and Y. B. Yang, "An effective means for damage detection of bridges using the contact-point response of a moving test vehicle," *Journal of Sound and Vibration*, vol. 419, pp. 158–172, 2018.

[35] W. Y. He, J. He, and W. X. Ren, "The use of mode shape estimated from a passing vehiclefor structural damage localization and quantification," *International Journal of Structural Stability and Dynamics*, vol. 19, no. 10, Article ID 1950124, 2019.

[36] Z. Hu, Z. Xiang, and Q. Lu, "Passive Tap-scan damage detection method for beam structures," *Structural Control and Health Monitoring*, vol. 27, no. 4, Article ID e2510, 2020.

[37] J. T. Li, X. Q. Zhu, S. S. Law, and B. Samali, "A two-step drive-by bridge damage detection using dual Kalman filter," *International Journal of Structural Stability and Dynamics*, vol. 20, no. 10, Article ID 2042006, 2020.

[38] A. Malekjafarian, P. J. McGetrick, and E. J. Obrien, "A review of indirect bridge monitoring using passing vehicles," *Shock and Vibration*, vol. 2015, Article ID 286139, 16 pages, 2015.

[39] X. Q. Zhu and S. S. Law, "Structural health monitoring based on vehicle-bridge interaction: accomplishments and challenges," *Advances in Structural Engineering*, vol. 18, no. 12, pp. 1999–2015, 2015.

[40] Y. B. Yang and J. P. Yang, "State-of-the-art review on modal identification and damage detection of bridges by moving test vehicles," *International Journal of Structural Stability and Dynamics*, vol. 18, no. 02, Article ID 1850025, 2018.

[41] Z. L. Wang, J. P. Yang, K. Shi, H. Xu, F. Q. Qiu, and Y. B. Yang, "Recent advances in researches on vehicle scanning method for bridges," *International Journal of Structural Stability and Dynamics*, vol. 22, no. 15, 2022.

[42] Y. B. Yang and K. C. Chang, "Extraction of bridge frequencies from the dynamic response of a passing vehicle enhanced by the EMD technique," *Journal of Sound and Vibration*, vol. 322, no. 4-5, pp. 718–739, 2009.

[43] E. J. Obrien, A. Malekjafarian, and A. Gonzalez, "Application of empirical mode decomposition to drive-by bridge damage detection," *European Journal of Mechanics - A: Solids*, vol. 61, pp. 151–163, 2017.

[44] J. P. Yang and W. C. Lee, "Damping effect of a passing vehicle for indirectly measuring bridge frequencies by EMD technique," *International Journal of Structural Stability and Dynamics*, vol. 18, no. 01, Article ID 1850008, 2018.

[45] L. Zhu and A. Malekjafarian, "On the use of ensemble empirical mode decomposition for the identification of bridge frequency from the responses measured in a passing vehicle," *Infrastructure*, vol. 4, no. 2, p. 32, 2019.

[46] Y. B. Yang, H. Xu, X. Q. Mo, Z. L. Wang, and Y. T. Wu, "An effective procedure for extracting the first few bridge frequencies from a test vehicle," *Acta Mechanica*, vol. 232, no. 3, pp. 1227–1251, 2021.

[47] Y. He, J. P. Yang, and Y. F. Li, "A three-stage automated modal identification framework for bridge parameters based on frequency uncertainty and density clustering," *Engineering Structures*, vol. 255, Article ID 113891, 2022.

[48] Y. B. Yang, Y. He, and H. Xu, "Automatically extracting bridge frequencies using SSA and K -means clustering from vehicle-scanned accelerations," *International Journal of Structural Stability and Dynamics*, vol. 22, no. 08, 2022.

[49] H. Q. Wang, T. Nagayama, J. Nakasuka, B. Y. Zhao, and D. Su, "Extraction of bridge fundamental frequency from estimated vehicle excitation through a particle filter approach," *Journal of Sound and Vibration*, vol. 428, pp. 44–58, 2018.

[50] H. Xu, C. C. Huang, Z. L. Wang, K. Shi, Y. T. Wu, and Y. B. Yang, "Damped test vehicle for scanning bridge frequencies: theory, simulation and experiment," *Journal of Sound and Vibration*, vol. 506, no. 18, Article ID 116155, 2021.

[51] H. Xu, Y. H. Liu, Z. L. Wang, K. Shi, B. Zhang, and Y. B. Yang, "General contact response of single-axle two-mass test vehicles for scanning bridge frequencies considering suspension effect," *Engineering Structures*, vol. 270, no. 5, Article ID 114880, 2022.

[52] S. S. Eshkevari and S. N. Pakzad, "Signal reconstruction from mobile sensors network using matrix completion approach," *Topics in ModalAnalysis & Testing*, vol. 8, pp. 61–75, 2020.

[53] Y. B. Yang, H. Xu, Z. L. Wang, K. Shi, and Y. T. Wu, "Refined detection technique for bridge frequencies using rocking motion of single-axle moving vehicle," *Mechanical Systems and Signal Processing*, vol. 162, Article ID 107992, 2022.

[54] H. Xu, Y. H. Liu, M. Yang, D. S. Yang, and Y. B. Yang, "Scanning and separating vertical and torsional-flexural frequencies of thin-walled girder bridges by a single-axle test vehicle," *Thin-Walled Structures*, vol. 182, Article ID 110266, 2023.

[55] Y. He and J. P. Yang, "Using Kalman filter to estimate the pavement profile of a bridge from a passing vehicle considering their interaction," *Acta Mechanica*, vol. 232, no. 11, pp. 4347–4362, 2021.

[56] J. Bayer and S. Urushadze, "Cogwheel load: a new forced vibration test for bridges?" *Journal of Civil Structural Health Monitoring*, vol. 12, no. 1, pp. 71–80, 2022.

[57] T. Nagayama, A. P. Reksowardojo, D. Su, and T. Mizutani, "Bridge natural frequency estimation by extracting the common vibration component from the responses of two vehicles," *Engineering Structures*, vol. 150, pp. 821–829, 2017.

[58] Y. B. Yang, Z. L. Wang, K. Shi, H. Xu, and J. P. Yang, "Adaptive amplifier for a test vehicle moving over bridges: theoretical study," *International Journal of Structural Stability and Dynamics*, vol. 21, no. 03, Article ID 2150042, 2021.

[59] J. D. Sitton, Y. Zeinali, D. Rajan, and B. A. Story, "Frequency estimation on two-span continuous bridges using dynamic responses of passing vehicles," *Journal of Engineering Mechanics*, vol. 146, no. 1, Article ID 04019115, 2020.

[60] Y. B. Yang, Y. H. Liu, and H. Xu, "Recovering mode shapes of curved bridges by a scanning vehicle," *International Journal of Mechanical Sciences*, vol. 253, Article ID 108404, 2023.

[61] Z. H. Shi and N. Uddin, "Theoretical vehicle bridge interaction model for bridges with non-simply supported boundary conditions," *Engineering Structures*, vol. 232, Article ID 111839, 2021.

[62] J. M. Biggs, *Introduction to Structural Dynamics*, McGraw-Hill, New York, NY, USA, 1964.

[63] S. Sadiku and H. H. E. Leipholz, "On the dynamics of elastic systems with moving concentrated masses," *Ingenieur-Archiv*, vol. 57, no. 3, pp. 223–242, 1987.

[64] R. W. Clough and J. Penzien, *Dynamics of Structures*, McGraw-Hill Book Co, Singapore, 1993.

[65] Iso, *Mechanical Vibration-Road Surface Profiles-Reporting of Measured Data*, International Organization for Standardization, Geneva, Switzerland, 1995.

[66] H. Xu, M. H. Wang, Z. L. Wang, D. S. Yang, Y. H. Liu, and Y. B. Yang, "Generation of surface roughness profiles for inclusion in vehicle-bridge interaction analysis and test application," *International Journal of Structural Stability and Dynamics*, 2022.

[67] R. G. Lyons, *Understanding Digital Signal Processing*, Prentice-Hall, Boston, MA, USA, 3rd edition, 2011.

[68] G. Warburton, "Optimum absorber parameters for various combinations of response and excitation parameters," *Earthquake Engineering & Structural Dynamics*, vol. 10, no. 3, pp. 381–401, 1982.

[69] A. Ghosh and B. Basu, "A closed-form optimal tuning criterion for TMD in damped structures," *Structural Control and Health Monitoring*, vol. 14, no. 4, pp. 681–692, 2007.

[70] N. Hoang, Y. Fujino, and P. Warnitchai, "Optimal tuned mass damper for seismic applications and practical design formulas," *Engineering Structures*, vol. 30, no. 3, pp. 707–715, 2008.

[71] M. Yahyai, L. Zebarjad, M. Head, and M. Shokouhian, "Optimum parameters for large mass ratio TMDs using frequency response function," *Journal of Earthquake Engineering*, vol. 25, no. 10, pp. 1–20, 2019.

[72] Y. B. Yang, M. C. Cheng, and K. C. Chang, "Frequency variation in vehicle–bridge interaction systems," *International Journal of Structural Stability and Dynamics*, vol. 13, no. 02, Article ID 1350019, 2013.